RSC Advances

ROYAL SOCIETY OF CHEMISTRY

www.rsc.org/advances

Cite this: DOI: 10.1039/c0xx00000x

www.rsc.org/xxxxxx

Full Paper

Mechanism Studies of $LiFePO_4$ Cathode Material: Lithiation/Delithiation Process, Electrochemical Modification and Synthetic Reaction

Feng Yu,[aef] Lili Zhang,[b] Yingchun Li,[c] Yongxin An,[d] Mingyuan Zhu,[a] and Bin Dai*[a]

Received (in XXX, XXX) Xth XXXXXXXXX 20XX, Accepted Xth XXXXXXXXX 20XX
DOI: 10.1039/b000000x

Olivine-structured lithium ion phosphate ($LiFePO_4$) is one of the most competitive candidates of energy-driven cathode material for sustainable lithium ion battery (LIB) systems. However, the high electrochemical performance is significantly limited by the slow diffusivity of Li-ion in $LiFePO_4$ (ca. 10^{-14} $cm^2 \cdot s^{-1}$) together with the low electronic conductivity (ca. 10^{-9} $S \cdot cm^{-1}$), which is the big challenge we are currently facing. To resolve the challenge, many efforts have been directed to dynamics of lithiation/delithiation process in Li_xFePO_4 ($0 \leq x \leq 1$), mechanism of electrochemical modification, and synthetic reaction process, which are all crucial for the development of high electrochemical performance for $LiFePO_4$ material. In this review, in order to reflect the recent progress ranging from very fundamentals to practical applications, we specifically focus on mechanism studies of $LiFePO_4$ including lithiation/delithiation process, electrochemical modification and synthetic reaction. Firstly, we highlight Li-ion diffusion pathway in Li_xFePO_4 and phase translation of Li_xFePO_4. Then we summarize the modification mechanism of $LiFePO_4$ with high-rated capability, excellent low-temperatured performance and high energy density. Finally, we discuss synthetic reaction mechanism of high-temperatured carbothermal reaction route and low-temperatured hydrothermal/solvothermal reaction route.

1 Introduction

As excellent electrochemical energy storage (EES) devices, lithium ion batteries (LIBs) have recently attracted significant attention, since the reversible lithiation/delithiation reaction of $LiCoO_2$ was discovered in 1980 and the use of $LiCoO_2$ as the cathode materials for LIBs in 1990.[1],[2] Compared to the conventional lead-acid, nickel-cadmium and nickel-metal hydride batteries, rechargeable LIBs possess high working voltage and superior energy density.[3],[4] LIBs are not only widely used in consumer electronics such as cell phones, cameras, toys and laptops, but also used to power increasingly emerging large-scale applications such as electric vehicles (EVs) and hybrid electric vehicles (HEVs).[5],[6] Nowadays, LIBs would facilitate the regulation of imbalance in electrical power grids and are closest to coupling ultimate requirement of advanced energy storage technologies for the renewable energy sources including solar power, wind and ocean waves.[7],[8] Noticeably, LIBs are timely meeting exigent demands of modern energy technology (ET), which is urgently needed to the thrust area closely linked to combustion engine and environmental pollution.[9],[10] Combined with renewable energy sources, LIB-based ET is an imperative step to replace the inevitably vanishing non-renewable fossil fuel and avoid negative effects from the current combustion-based ETs on global energy and environmental problems.[11],[12] LIBs have become the most viable and promising candidates for EES devices, which strongly minimize environment impact and maximize energy and resources utilization.[13],[14]

Although LIBs are well positioned to satisfy the needs of modern society and emerging ecological concerns, one of the greatest challenges is unquestionably the cathode materials where the Li-ions extracting/inserting process occured.[15],[16] Scientists have been focus on the crystal structures and the electrochemical performance of potential cathode materials, such as olivine-structured $LiMPO_4$ (M=Fe, Co, Ni, Mn), α-$NaFeO_2$ layered $LiMO_2$ (M=Co, Ni, Mn), monoclinic structured $Li_{1+x}V_3O_8$, orthogonal structured Li_2MSiO_4 (M=Fe, Mn), spinel structured $LiMn_2O_4$ and NASCION structured $Li_3V_2(PO_4)_3$.[17],[18] Among aforementioned cathode materials, layer-structured $LiCoO_2$ with two-dimensional (2D) Li-ion transport has been extensively utilized in LIBs. However, it suffers from high toxicity, inferior safety and high cost.[19] Recently, cubic-spinelled $LiMn_2O_4$ supporting three-dimensional (3D) Li-ion transport has also been widely used in high powerful EES devices. However, its poor cycle life due to the Jahn-Teller effect remains a bing concern.[20],[21]

Thanks to the groundbreaking work conducted by Goodenough and co-workers,[22],[23] phosphate polyanionic

compound $LiFePO_4$ has attracted tremendous attention and has been used as cathode material in LIBs because of its fantastic performance, such as high theoretical capacity (170 $mAh \cdot g^{-1}$), acceptable operating voltage (3.45V vs. Li^+/Li), long cycle life (>2000 cycles), superior safety, low cost, low toxicity, abundant resources, and environmental benign.[24],[25] In the orthorhombic olivine-structured $LiFePO_4$, the oxygen atoms are located in a hexagonal close-packed and slightly distorted arrangement.[26],[27] The phosphorus atoms are on tetrahedral sites and forming PO_4 tetrahedra with oxygen atoms. Lithium atoms from LiO_6 octahedra occupy edge-sharing octahedral positions, while iron atoms from FeO_6 octahedra occupy corner-sharing octahedral positions. Due to the edge-sharing chains along the [010] direction (i.e., b-axis) created by the LiO_6 octahedra, one-dimensional (1D) Li-ion transport is formed in the [010] direction. At the common corners in the bc plane, one FeO_6 octahedron is chained with four FeO_6 octahedra resulting in zigzag planes parallel to the [001] direction (i.e., c-axis). Each FeO_6 octahedron shares one edge with PO_4 tetrahedra and two LiO_6 octahedra, respectively, while PO_4 tetrahedra has two common edges with LiO_6 octahedra.[28] This special olivine-structured $LiFePO_4$ gives great niches including excellent structural flexibility and superior thermal stability, and provides excellent cycling capabilities and safe characteristics superior to other cathode materials.[29],[30],[31]

However, there are some limitations of high rate capability due to simplex 1D Li-ion transport of the olive-structured $LiFePO_4$, which is different from the layer-structured $LiCoO_2$ providing 2D Li-ion transport and the cubic-spinelled $LiMn_2O_4$ supporting 3D Li-ion transport.[18],[32] Its high-rate performance is significantly limited by the slow diffusivity of the Li-ion in $LiFePO_4$ (ca. 10^{-14} $cm^2 \cdot s^{-1}$) together with the low electronic conductivity (ca. 10^{-9} $S \cdot cm^{-1}$).[23],[33] The poor power density of $LiFePO_4$ cathode for LIBs limits its application in power-demanding EVs and HEVs.[15],[34] The development of cathode materials for LIBs with high-rate capability, low-temperature performance, good cycle life and high energy density are still challenging. Efforts have been devoted to the understanding of the dynamics of the lithiation/delithiation process Li_xFePO_4 ($0 \leq x \leq 1$), the electrochemical reaction mechanism, and optimization of synthetic approach, which are crucial for the development of high performance $LiFePO_4$ material.

In this review, we highlight the mechanism studies of $LiFePO_4$ including lithiation/delithiation process, electrochemical property modification and synthetic approach, which are necessary to fully employ its great potential for practical applications. Firstly, we introduce Li-ion diffusion pathway in Li_xFePO_4 and phase translation of Li_xFePO_4 to provide fundamentals for the development of high electrochemical performance $LiFePO_4$ material. Secondly, we focus on the crucial parameters representing the performances of $LiFePO_4$, which mainly include specific capacity, rate capability, tap density and low temperature performance. Comprehensive improvements of all those parameters are desired and are also the targets for future research. Finally, we discuss the synthetic reaction mechanism of carbothermal reaction (CTR) route and hydrothermal/solvothermal reaction route, which are two of the most important synthesis routes that need to be improved urgently. We believe this review not only benefits the research of $LiFePO_4$, but also provides an additional strategy for other materials potentially used in EES devices.

2 Lithiation/delithiation process in $LiFePO_4$

2.1 Li-ion diffusion pathways of $LiFePO_4$

2.1.1 One-dimensional Li-ion diffusion along [010] direction

Owing to the quite compact olivine structure, $LiFePO_4$ exhibits intrinsic thermal stability in the fully charged state, which makes a major contribution to LIBs safety. Moreover, $LiFePO_4$ presents excellent structural flexibility, which provides remarkably good cycling stability compared with cathode materials. However, there are still some obstacle and limitations of its high rate capability. Thus, it has been critical to explore Li-ion diffusion pathway and explain phase transition during the lithiation/delithiation process of $LiFePO_4$.[27],[35] In recent years, first principle-based modeling has become an important tool to study reaction in charge and discharge. In 2004, Ceder and his co-workers[36] firstly employed first-principles method to study Li-ion transport direction in $LiFePO_4$. They demonstrated that Li-ion diffusion coefficient was successfully calculated to be several orders of magnitude higher in the [010] direction (i.e. b-axis) than in the [001] direction (i.e. c-axis). The result of $D_{[001]}/D_{[010]} \approx 10^{-37}$ clearly shows that [001] direction hardly makes contribution to the Li-ion motion. Li-ion diffuses through 1D channels along [010] direction with low energy barriers to cross between the channels due to the FeO_6 octahedral transition state in [001] direction being face-sharing with two PO_4 tetrahedra. Islam's group[26],[37] further designed the structural modeling of $LiFePO_4$ and used atomistic simulation method to investigate Li-ion migration energy in $LiFePO_4$. They found that the energy of Li-ion migration is $E_{mig}([010])=0.55$ eV lower than $E_{mig}([001])=2.89$ eV and $E_{mig}([101])=3.36$ eV, which strongly indicates a preference for Li-ion transport along the [010] direction and confirmes results of Ceder's group. Some more theoretical calculations have also been reported and suggested that Li-ion transport is along [101] direction due to the lower Li-ion migration energy than other directions.[38],[39]

Moreover, Li-ion migration was preferential down [010] channels following a curved trajectory, which is confirmed by Yamada's group.[40] As shown in Fig.1, ellipsoids representing Li-ions were refined with 95% probability by Rietveld analysis and motions of Li atoms evolve from vibration to diffusion as an expected curved one-dimensional continuous chain. Moreover, Tse's group[41] found that Li-ion diffusion is a dominant process trough a series jumps from one site to another, resulting into a zigzag pathway along the crystallographic [010] direction. As mentioned above, the Li-ion diffusion pathway mainly occur in [010] direction, which creates simplex one-dimensional Li-ion transport pathway and is different from that of 2D layer-structured $LiCoO_2$ and 3D cubic-spinelled $LiMn_2O_4$. 1D Li-ion transport tunnel is considered as the main cause of slow Li-ion diffusion, which significantly restricts the high rate performance of $LiFePO_4$.[42]

In order to experimentally prove whether Li-ion diffusion

pathway is one-dimension along [010] direction, ionic conductivity (or ionic mobility) is generally measured and used to calculate ionic diffusivity. Various techniques including cyclic voltammetry (CV), galvanostatic intermittent titration technique (GITT), potentiostatic intermittent titration technique (PITT), electrochemical impedance spectroscopy (EIS), *etc*., can be used to measure ionic conductivity under applied voltage.[43] Vaknin's group[44] employed AC impedance spectroscopy to study the Li-ion conductivity of three principal directions (i.e. [100], [010] and [001]) in single crystal $LiFePO_4$ as a function of temperature (325-525 K). Their results indicate that ionic conductivity along the [010] direction is much higher than that in both [100] and [001] direction, which agrees well with computational analysis. Meanwhile, Yamada's group[40] provided clearly experimental visualization of Li-ion transport Li_xFePO_4 (x=0.6) by combining high-temperature (620 K) powder neutron diffraction and the maximum entropy method (MEM), as shown in Fig.1b, 1c and 1d. To a large extent, lithium delocalizes along the continuous curved 1D chain along the [010] direction on account of the probability density of lithium nuclei. The result is consistent with the aforementioned computational predictions. Therefore, the lithium diffusion constant in nanoparticles with shortened transport paths is much faster than that in bulk.[45]

2.1.2 Two-dimensional Li-ion diffusion along both [010] and [001] directions

Second possible direction of Li transport has been postulated due to the chains separated by octahedral interstitial sites along the [001] direction at elevated temperature, which suggest that 2D Li-ion transport exist along both [010] and [001] directions.[23],[46] As shown in Fig.2a, Maier's group[47] investigated ionic and electronic conductivity in single crystalline $LiFePO_4$ as a function of crystallographic orientation over an extended temperature range, and found that activation energies obtained for ionic conductivities σ_{Li}+ along [010] and [001] orientations are (i.e., $E_{act}([001])=E_{act}([010])=0.62$ eV) smaller than that of [100] direction (i.e., $E_{act}([100])=0.74$ eV), which is corresponding to an effectively two-dimensional Li^+ conduction. In addition, their study suggested that activation energies presented for Li-ion diffusion DLi^{δ} along [010] and [001] direction are comparable (i.e., $E_{act}([001])=0.75$ eV, $E_{act}([010])=0.70$ eV) distinctly less than that of [100] direction (i.e., $E_{act}([100])=0.96$ eV) (see in Fig.2b), which indicated a preferential 2D Li-ion chemical diffusion in the b-c plane. The phenomenon accounted for effective two-dimension of Li-ion conductivity and diffusion (i.e., isotropic in the b-c plane). Their study suggested that the ionic conductivity magnitudes in both the [010] and [001] directions and the diffusion coefficient are the similar at the temperature of 140-147 ^oC, indicating that 2D Li-ion transport must occur at that temperature.

Furthermore, Nazar's group[48] has also reported that the small polar on carrier mobility is predicted to be "two-dimensional" with motions of Li ions as well as electrons being correlated using Mössbauer spectroscopy measurement. They gave experimental evidence for a strong correlation between electron and lithium delocalization events suggesting they are coupled. In 2011, Henkelman's group[49] reported the various components of Li-ion kinetics in $LiFePO_4$ calculated from density functional theory (DFT). As shown in Fig.2c, there are different kinetic pathways of Li-ion diffusion on the surface, in the bulk, in the presence of defects, and in varying local environments. It is observed that surface diffusion had high barriers resulting into slow kinetics in $LiFePO_4$. Moreover, the slow bulk diffusion was possibly affected by strain and Li concertration. The slow vacancy diffusion in $LiFePO_4$ was explained by anti-site defects, which has a barrier of 0.71 eV (Fig.2d) compared to 0.29 eV in defect-free channels. Intriguingly, a concerted Li-ion diffusion in $FePO_4$ exhibited a low barrier of 0.35 eV, allowing for facile cross-channel diffusion at room temperature.

2.2 Phase transition between $LiFePO_4$ and $FePO_4$

2.2.1 Two-phase transformation between $LiFePO_4$ and $FePO_4$

The lithiation/delithiation process in Li_xFePO_4 ($0\leq x\leq 1$) is commonly proposed as a two-phase reaction mechanism, which includes various models: shrinking core (i.e., core–shell) model,[23],[50] Laffont's (i.e., new core-shell) model,[51] mosaic model,[52],[53] domino-cascade model,[54],[55] phase transformation wave model,[56],[57] and many-particle model.[58] Generally, two-phase growth process involves the coexistence of $LiFePO_4$ and $FePO_4$, particlully for the large particles (e.g., particle size > 100 nm).

In 1997, Goodenough's group[23] firstly reported that Li-ion exhibited a two-phase transport between $LiFePO_4$ and $FePO_4$ due to the flat charge/discharge profile, and introduced "core-shell" model. With delithiation, $LiFePO_4$ change into $FePO_4$, and become two phases and a two-phase interface. This model is generally named "core-shell" model. This model can explain the reaction, However, it can not explain the continuous deviation of the open circuit voltage (OCV) from 3.45 V at the initial start and the end of the discharge. Subsequently, Srinivasan's group[50] proposed a "shrinking core" model to describe the lithiation of $FePO_4$. This model showed that outside the two-phase coexistence region there would be a corresponding single phase region, where lithiation proceeds from the surface of a particle moving the two phase interface. With delithiation in charging process, $FePO_4$ shell formed and the $FePO_4/LiFePO_4$ interface migrated into each particle. Unefficient delithiaiton from the uncovered $LiFePO_4$ at the center of the larger particles easily leads to the capacity loss. Simultaneously, this shrinking-core model can successfully describe electrochemical charge/discharge profiles at various rates.[59]

Similar to the shrinking-core model, Thomas's group[52],[53] proposed a "mosaic model" by introducing a new concept, i.e., lithiation/delithiation starting at different nucleation sites. These two models are generally considered as "the conventional two-phase mechanism". However, these two models do not take into account any anisotropy arising from the 1D Li-ion motion within $LiFePO_4$, which is powerless to describe the lithiation/delithiation process in $LiFePO_4$. Otherwise, the "mosaic model" is still not supported by the direct and convincing experimental evidence.

Laffont's group[51] and Richardson's group[60] found that the interfacial region between the $LiFePO_4$ and $FePO_4$ domains lie in the a-c plane (see in Fig.3). Then Laffont's group[51] updated the "core-shell" model and proposed a "new core-shell" model based on studies of thin Li_xFePO_4 platelets (b-axis normal to the

surface) with high resolution electron energy loss spectroscopy (HREELS). Different from the previous shrinking core model, the results suggested that the interface is constituted of $FePO_4$ and $LiFePO_4$. There is no Li_xFePO4 solid solution observed with gradient of x ranging from 0 to 1. The schematic views of the interfacial region between $LiFePO_4$ and $FePO_4$ phases are provided in Fig.3. According to this new core model, Li-ion diffusion in [010] direction is asynchronous, and the Li_xFePO_4 particles always keep the structure with shell of $FePO_4$ and core of $LiFePO_4$, as has also been suggested by Prosini's group.[61] Moreover, this new core shell model is unambiguously supported by Lemos's group[62] who observed the existence of both $FePO_4$ and $LiFePO_4$ phases at the interface of $Li_{0.11}FePO_4$.

However, Delmas' group[54],[55] found that the interface consisted of a single-domain of Li_xFePO_4 rather than $LiFePO_4$ and $FePO_4$. Based on the results from X-ray diffraction (XRD) and high resolution transmission electron microscope (HRTEM), a "domino-cascade" model was successfully established to explain phase transformation process of $LiFePO_4$ nanoparticles. The results illustrated that the growth of $FePO_4$ phase at the expense of the $LiFePO_4$ phase is considerably faster than the nucleation of new domain. According to the "domino-cascade" model, lithiation/delithiation totally carried out rapidly in some of the $LiFePO_4$ nanoparticles with charing/discharging. Thus, the partially intercalated/de-intercalated $LiFePO_4$ particle generally supported the coexistence of $LiFePO_4$ and $FePO_4$ particles that are single-domain.

In 2013, Zhou's group[63] studied the phase transition in Li_xFePO_4 by electrochemical impedance spectroscopy (EIS) and firstly proposed a hybrid phase-transition model combining the core-shell model and demino-cascade model. Based on this model, the delithiation of Li_xFePO_4 starts with the demino-cascade model confirmed by a samll angel of 30° for the linear Warburg region of EIS, and then turn into core-shell model approved by a traditional angel of 45°. This hybrid phase-transition model gives attributions to the strong anisotropy in the Li_xFePO_4 particles and could be potentially extended to some other two-phase active electrode materials.

Recently, a "many-particle model" has also been provided. Gaberscek's group[58] found that Li-ions were inserted/extracted from $LiFePO_4$ particles one by one forming a two-phase system. Meanwhile, Zaghib's group[64] found that both of $LiFePO_4$ and $FePO_4$ phases exist in the surface layer by using electron microscopy and Raman spectroscopy. This is intended to explain the fact that the lattice coherence length is the same in the process of lithiation/delithiation while invalidates both core-shell model and the domino-cascade model. Each particle would be single-phased, either $FePO_4$ or $LiFePO_4$, which explain how one particle chooses to be in one phase while another one remains in the other phase without violating the causality principle. Subsequently, Orikasa group[65] observed transient phase change in two phase reaction during lithiation/delithiation process by applying the time-resolved X-ray measurement. It is found that the nonequilibrium phase state during the voltage plateau gradually changes and finally reaches the thermodynamical stable state by the analysis X-ray absorption near edge structure (XANES).

Basd on the observation and demonstration by Delamas' group[54] and Ceder's group[45], Chueh's group[66] also observed the overwhelming majority of $Li_{0.5}FePO_4$ particles (i.e., $LiFePO_4$ electrode in 50% state-of-charge) were either almost completely delithiated $LiFePO_4$ particles or lithiated $FePO_4$ particles in 2013. With the help of scanning transmission X-ray microscopy (STXM), it is clearly found that the delithiation did not appear faster in smaller particles than larger ones resulting into a weak correlation between the particle size and delithiation sequence. Therefore, the mosaic (particle-by-particle) lithiation/delithiation pathway indicated that rate performance was limited by the rate of phase-transformation initiation rather than the phase-boundary velocity. Moreover, the model can be used to predict the equilibrium between $LiFePO_4$ and $FePO_4$ phases, inherent hysteretic behaviour, sequential charging/discharging mechanism and two-phase disappearance behaviour. Porous $LiFePO_4$ electrodes were also investigated by Bai's group[67] using a mathematical phase-field method. It is found that the population dynamics of active $LiFePO_4$ nanoparticles showed non-monotonic transient currents always misinterpreted as the nucleation and growth mechanism by the Kolmogorov-Johnson-Mehl-Avrami (KJMA) theory. The $LiFePO_4$ nanoparticles were not simultaneously transformed. The results decoupled the roles of nucleation and surface reaction, which always considered to be affected by a special activation rate and the mean active particle-filling speed. Ichitsubo's group[68] also applied the phase-field computer simulations to investigate the coherent elastic-strain energy which played a curcial role in the kinetics of phase separation during lithiation/delithiation process. However, it is found that nucleation the new phase is fundamentally unlikely formed in therms of the elastic strain energy except in the vicinity of the particle surface. The simulation results illustrated that the solid-solution reaction easily occurred by reducing the particle size, but the phase separation by nucleation is quite difficult to carry out. Meanwhile, Dargaville' group[69] employed the 2D Cahn-Hilliard-reaction (CHR) equation to examine intercalation process and suggested that the phase separation only occurred at very low discharge rates.

All these aforementioned models are expected to understand the lithiation/delithiation process in $LiFePO_4$, and provide directions to improve rate capability of $LiFePO_4$ for high power EES applications. However, these models invalidate each other and are still under debate. Nevertheless, it is still unclear whether the staging phenomenon refers to a thermodynamically metastable or stable situation in Li_xFePO_4 nanoparticles. Theoretical and experimental and theoretical clarification should be further undertaken to clarify the formation mechanism of the lithium staging. Thus, as mentioned above, a single unified model is urgently required to depict the natural lithiation/delithiation process in Li_xFePO_4, and a computational model of lithiation/delithiation process in $LiFePO_4$ is essential to clarify the above question. Compared with conventional generalized gradient approximation (GGA)[70],[71] and local-density approximation (LDA) methods,[72],[73] GGA+U method can avoid large errors especially for transition metals with strong localized or f-orbitals metals and can well improve the results.[74],[75],[76] In the future, we anticipate that the lithiation/delithiation process in $LiFePO_4$ will be simulated by computational model using GGA+U method. This natural model not only offers answers to experimental results obtained at moderate or high rates, but also

gives the direction to prepare $LiFePO_4$ for high power LIBs.

2.2.2 Quasi-single-phase transformation between $LiFePO_4$ and $FePO_4$

Different from two-phase reaction mechanism models, quasi-single-phase transformation between $LiFePO_4$ and $FePO_4$ has also attracted much attention. It is doubt that an intermediate phase existing during the lithiation/delithiation process of Li_xFePO_4. In 2011, Li's group[77] directly observed Li-ions in $LiFePO_4$ were at atomic resolution by an aberration-corrected annular-bright-field scanning transmission electron microscopy (ABF-STEM) technique (Fig.4a), which is capable of resolving Li-ions directly. It was found that the remaining Li-ions in partially delithiated $LiFePO_4$ preferably occupy every second layer, along the [010] direction (i.e., b axis) (Fig.4b and 4c). Obviously, this finding challenged previously proposed $LiFePO_4/FePO_4$ two-phase reaction mechanisms. In 2011, Ceder's group[78] demonstrated that Li_xFePO_4 may transform through a single-phase path instead of two-phase progress. As shown in Fig.4d, the calculated single-particle voltage hysteresis is no more than 30 mV, where $0.05<x<0.9$ in Li_xFePO_4. It is clearly shown that the Li_xFePO_4 solid solution formed and avoided phase separation in charging and discharging process. Solid-solution behavior in the Li_xFePO_4 system is also observed by Richardson's group via X-ray powder diffraction (XRD).[79] In the $Li_{0.6}FePO_4$ sample, there was an intermediate of a line phase with Li_xFePO_4 ($x= 0.60 \pm 0.04$) composition during the transformation from two-phase mixtures to single phase. In 2011, Bazant's group[80] proposed a novel electrochemical phase-field model. Based on the model, nucleation or spinodal decomposition easily leads to moving phase boundaries at small currents, whereas particles fill homogeneously and spinodal disappears above a critical current density, as shown in Fig.5. This model can effectively explain long cycle life and superior rate capability of $LiFePO_4$ nanoparticles.

Recently, single phase of solid solution Li_xFePO_4 has been found at high temperature above 200 ^oC.[81] As shown in Fig.4e, Nazar's group[48] found that single Li_xFePO_4 solid solution phase formed at elevated temperature of 212 ^oC and the lithiation/delithiation process were strongly enhanced. Owing to the single phase, the electrochemical performance is improved by a strong coupled correlation between electron and lithium delocalization events, whereas the power characteristics could be diminished in a two-phase mixture on account of low mobility of the phase boundary. All these results are in good agreement with the report of Masquelier's group,[82],[83] who found that the single phase of the Li_xFePO_4 become multiphase as the temperature decrease and eventually transformed into the phases of $LiFePO_4$ and $FePO_4$ on aging at room temperature.

Excitedly, Masquelier's group[84],[85] provided an in-situ experimental evidence that Li_xFePO_4 can be described as single phase from well-established two-phase lithiation process by modify the particle size and cation ordering. It is can be found that the single intermediate phases of $Li_{0.5}FePO_4$ and $Li_{0.75}FePO_4$ might be stabilized at room temperature. Simultaneously, the Li_xFePO_4 solid solution may be stabilized below critical size of 45 nm, and completely achievable below about 15 nm at room temperature.[86] It is worth mentioning that the lithiation/delithiation mechanism is still in the controversy and attract more and more attention. A series of conditions including particle morphologies, synthesis conditions, charge/discharge rates, especially state particles size, are still be debated.[87],[88]

3 Electrochemical property modification of $LiFePO_4$

The $LiFePO_4$ delivers high capacities more than 150 $mAh\cdot g^{-1}$ at slow charging/discharging rates (e.g., 0.1 C). However, high-rated charge/discharge properties and low temperature performance are severely limited due to the poor electronic conductivity and the low Li-ion diffusion efficicency. Namely, electronic conductivity and ionic diffusion rate are two of the most important characteristics that need to be improved urgently. It is demonstrated to enhance the Li-ion diffusion by controlling crystal growth orientation (along the a-c plane) and reducing the particle size of $LiFePO_4$ (e.g., nano-sized[89],[90] and 3D porous architectures[91],[92]). It is also important to ensure an excellent electronic conductivity by coating conductive materials (e.g., amorphous carbon,[93],[94] graphene,[95] carbon nanotubes (CNTs),[96] silver,[97] NiP alloy,[98] metallic Fe_2P,[99],[100] Li_3PO_4,[101] etc.). Both ionic diffusion and electronic conductivity can be employed to improve the kinetic properties of $LiFePO_4$ by doping in M_{Li} and M_{Fe} sites using cations of metallic elements (e.g., Cu^+, Mg^{2+}, Mn^{2+}, Al^{3+}, Ti^{4+}, Zr^{4+}, Nb^{5+}, W^{6+}, *etc.*).[62],[102],[103] Comprehensive improvements of all effective strategies are desired and are also the targets for the high-rated charge/discharge properties and low temperature performance, which are two important parameters for future research and EES applications (especially for EV/HEV). Moreover, volume energy density of $LiFePO_4$ is another important parameter, which is critical to maximizing space utilization of LIBs. In the following section, we will introduce representative reports on how to improve the performances of $LiFePO_4$. The reports are categorized into the improvement of (a) rate capability, (b) low temperature performance and (c) tap density.

3.1 Morphology control

3.1.1 Crystal growth orientation along the a-c plane

The Li-ion diffusion rates vary along different directions in $LiFePO_4$ lattices. If we can deliberately control the synthesis of $LiFePO_4$ crystals with certain exposed facets for faster Li-ion intercalation, the performances especially rate capabilities can be significantly improved. Previous reports showed that Li-ion diffused fastest along [010] direction in the orthorhombic $LiFePO_4$ lattice.[40] Islam's group[104] revealed that there were mainly three crystal styles agreeing with the results from Franger's group[105], Nazar's group[106] and Richardson's group[60], as shown in Fig.6a-d. The crystal growth of anisotropic cathode $LiFePO_4$ is addressed as a key factor controlling rapid Li-ion diffusion. Several surface properties of olivine-structure $LiFePO_4$ were investigated via first principles calculations within the GGA+U framework by Ceder's group.[107] The calculated Li redox potential for the (010) surface was 2.95 V, which is significantly lower than the bulk value of 3.55 V. The study revealed that it is important to control morphology of $LiFePO_4$ crystal growth orientation and expose more surface of (010) with high Li^+ diffusion rate.[108] Thus, if $LiFePO_4$ crystals are

fabricated with more (010) facets, such as thin nanoplates with (010) surfaces, superior performances can be expected due to the fast Li^+ insertion and extraction. Richardson's group[60] reported the hydrothermal synthesis of $LiFePO_4$ microcrystals with 85% (010) surface areas, but no electrochemical testing was performed. Further improvements, like synthesis of smaller and thinner nanoplates with more (010) surfaces, coating with conductive carbon layer may be considered to fully explore the potential of those nanoplates.[109]

In 2011, a combination of $LiFePO_4$ rectangular nanoplates was prepared by a low temperature solvothermal synthesis (STS) route reported by Kim's group,[110] as shown in Fig.6e. It can be seen that the growth of the $LiFePO_4$ nanoplates is identified to be along [100] and [010] crystallographic directions, resulting into large surface area of (001) rather than (010). Thus, the as-prepared $LiFePO_4$ nanoplates performed first discharge capacity of only 131 $mAh\cdot g^{-1}$ at 0.25 C (Fig.7), on account of the relatively low (101) surface area. Especially, the as-prepared $LiFePO_4$ nanoplates exhibited a capacity decline of about 38 $mAh\cdot g^{-1}$ until 8 C. Wang's group and Wu's group,[111] found that the obtained $LiFePO_4$/C composite exhibited high rate capability using carbon coating and performed 104 $mAh\cdot g^{-1}$ and 95 $mAh\cdot g^{-1}$ at 8 C and 12C, respectively.

Fig.6f shows $LiFePO_4$ hexagonal nanoplates (100 nm thick and 800 nm wide) prepared by a solvothermal method in a H_2O-PEG binary solvent.[112] Compared with $LiFePO_4$ hexagonal microplates (300 nm thick and 3 mm wide), carbon coated $LiFePO_4$ nanoplates exhibited the calculated Li-ion diffusion coefficient of 4.2×10^{-9} $cm^2\cdot S^{-1}$ instead of 2.2×10^{-9} $cm^2\cdot S^{-1}$, and delivered a discharge capacity more than 155 $mAh\cdot g^{-1}$ instead of 110 $mAh\cdot g^{-1}$ at 0.1 C. Particularly, $LiFePO_4$/C nanoplates could performed a high discharge capacity of 87 $mAh\cdot g^{-1}$ at 60C (i.e., fully discharged within 30 s), when the content of conductive carbon was increased to 30 wt.%.

Recently, Balaya and co-workers[113],[114],[115] employed a solvothermal method to control crystal growth orientation along the a-c plane and reduce the b-axis to the smallest possible thickness. As shown in Fig.6g and 6h, the thickness along the b-axis of $LiFePO_4$ nanoplates is found to be 30-40 nm, while the thickness along a-c plane is in the range 500-800 nm. The selected area electron diffraction (SAED) pattern viewed along [010] (i.e., b-axis) reveals that the plate is a single crystal with the b-axis along the thinnest direction. It is indicated that the smallest dimension of the nanoplates is the b-axis, which is propitious to diffusion of the Li-ions.[112] The as-obtained $LiFePO_4$/C nanoplates could store Li-ions comparable to its theoretical capacity of 87 $mAh\cdot g^{-1}$ at 0.1C. Even at 30C, they could delivered discharge capacity up to 87 $mAh\cdot g^{-1}$. All the results revealed that the excellent high rate performance of $LiFePO_4$ nanoplates is ascertained to the relatively thin thickness along the b-axis and large (101) surface area. In other words, size reduction (similar to 30 nm) at the b-axis and crystal growth orientation along the a-c plane could provide fast Li-ion diffusion. Moreover, uniform carbon coating (similar to 5 nm) throughout the $LiFePO_4$ nanoplates favors electronically conducting path for electrons.

3.1.2 Nano-sized $LiFePO_4$ particles

To date, the most widely adopted strategy to improve the rate capability is to use $LiFePO_4$ structures with smaller sizes and coat the structures with carbon to improve the electronic conductivity.[108] Particularly, nano-structured $LiFePO_4$ particles are in favor of reducing the 1D diffusion length and advantageous for Li-ions transport, as the intrinsic diffusion constant is scale dependent and significantly reduced at large particle size.[45] Various carbon-modified $LiFePO_4$ nanostructures have been studies, such as nanoparticles, nanorods, nanoflowers, porous microspheres, nanoplates, nanowires/fibers, template mesoporous materials, *etc*.[116] Smaller structures mean shorter diffusion path for Li-ion and hence better utilization of the active materials.[117] For example, assuming that for a certain time Li-ion can diffuse 50 nm within $LiFePO_4$ lattices, if the electrode is made of a single crystal $LiFePO_4$ film with a thickness of 1 mm, then only the 50 nm on the surface can be utilized. However, if the electrodes are made of nanoparticles below 100 nm diameters and proper electrolyte wrapping and electron conduction is ensured, the entire nanoparticle and hence electrode materials can be utilized.[118] This is why nanosized materials are favored for high specific capacity and high rate capability.[119],[120] As discussed above, at a high charge/discharge rate, less time is allowed for the ion diffusion. Consequently, nanostructures maintain a better capability for complete "reactions" with Li-ion within a short time. These nano-sized $LiFePO_4$ materials could provide short diffusion length, give better rate performances than bulk materials because of smaller diffusion length, and be beneficial for Li-ion batteries, as shown in Fig.8a.

Ball milling method is usually employed to synthesize nano-sized $LiFePO_4$/C composite. It is found that $LiFePO_4$/C from ball milling in acetone displayed spherical shape with a size of 60 nm, similar to the size of $LiFePO_4$/C observed from dry ball milling (DBM) but with a more irregular morpholog.[121] Although the $LiFePO_4$/C nanocomposites prepared from wet ball milling (WBM) in acetone and DBM exhibited the similar discharge capacities of 153 $mAh\cdot g^{-1}$ and 120 $mAh\cdot g^{-1}$ at rates of 0.1C and 10 C, respectively (Fig.9a), the previous sample performed much lower polarization resulting in high energy density. A core-shell structured $LiFePO_4$/C nanocomposite was also successfully designed and prepared by Zhou's group.[122] An *in-situ* polymerization restriction method was firstly used for the synthesis of $FePO_4$/PANI. Then a highly crystalline $LiFePO_4$ core was formed with a size of about 20-40 nm, and the polymer shell was transformed into a semi-graphitic carbon shell with a thickness of about 1-2 nm during the heat treatment process at 700 ^oC, as shown in Fig.8b. The as-obtained $LiFePO_4$/C performed excellent rate performance. Even at the high rate of 60C, it still delivered a capacity of 90 $mAh\cdot g^{-1}$. Additionally, Cho's group[123] reported $LiFePO_4$ nanowires were synthesized using the two-dimensional hexagonal SBA-15 silica as hard template. The $LiFePO_4$ nanowires delivered excellent rate performance. Even at 10C and 15C, The $LiFePO_4$ nanowires showed 144 $mAh\cdot g^{-1}$ and 137 $mAh\cdot g^{-1}$ respectively, corresponding to 93% and 89% capacity retention of the initial capacity.

Taniguchi's group[124] employed a combination technique of spray pyrolysis (SP) with WBM to prepared $LiFePO_4$/C nanoparticles. It is found that the $LiFePO_4$/C nanoparticles processed a geometric mean diameter of 146 nm. A thin carbon layer provided $LiFePO_4$ excellent electrochemical performance,

because $LiFePO_4$ nanoparticles exhibited an extremely high stability with the carbon coating.[125] The $LiFePO_4$/C showed 118 $mAh\cdot g^{-1}$ and 105 $mAh\cdot g^{-1}$ at 10C and 20C, respectively. Even at 60C, the $LiFePO_4$/C also performed 75 $mAh\cdot g^{-1}$ without capacity fading after 100 cycles. Amazingly, Ceder's group[126] found $LiFe_{1-2y}P_{1-y}O_{4-\delta}$/C (y=0.05) nanoparticles prepared by WBM in acetone exhibited outstanding high rate performance. The $LiFe_{0.9}P_{0.95}O_{4-\delta}$/C off-stoichiometry nanoparticles showed a specific discharge capacity of 163 $mAh\cdot g^{-1}$ and $mAh\cdot g^{-1}$ at 10C and 20C respectively. Significantly, the specific capacity still remains above 120 $mAh\cdot g^{-1}$ at a discharge rate as high as 197 C, when changing the woring electrodes fabrication of active material, carbon black and binder in a weight ratio of 80:15:5 to 30:65:5. This result is a remarkable progress over previous studies. This presents a new direction on the improvement of LFP cathode performances, although more work are needed to further improve the repeatability and mechanism understandings of this method.

3.1.3 Three-dimensional porous architectures with micro-nano structures

3D porous $LiFePO_4$ materials not only enhance surface-to-volume ratio and reduce Li-ion transport length, but also offer a potential solution to reduce interfacial energy and agglutinant in electrode, all of which are much better than those measured for the nano-sized $LiFePO_4$ and hollow micro-spherical $LiFePO_4$ (Fig.8c), improve the electrochemical performance and practical applications of $LiFePO_4$.[123],[127] Particularly, $LiFePO_4$ cathodes with 3D porous architectures, spherical architectures, and micro-nano-structures have been extensively and intensively studied for high powerful LIBs. With the aid of template technology, a variety 3D porous $LiFePO_4$ materials have been synthesized.[128],[129],[130] In 2013, Zhang's group[131] successfully prepared 3D mesoporous $LiFePO_4$ using Baker's yeast cells both as a structural template and a biocarbon source. The as-obtained $LiFePO_4$ exhibited a high discharge capacity of about 153 $mAh\cdot g^{-1}$ at 0.1 C.

Besides the soft template, Li_3PO_4/graphene oxide (GO) microspheres are also employed as sacrificial templates to synthesized porous $LiFePO_4$/graphene microspheres.[132] The as-obtained $LiFePO_4$/graphene microspheres (2 μm) were assembled by nanoparticles and wrapped by graphene nanosheets. The graphene has been proved an advantage for EES application on accont of the superior electrical conductivities and high surface area. Moreover, the porous microsperical structure exhibited an effective way to achieve high power density for $LiFePO_4$. The as-obtained $LiFePO_4$/graphene performed excellent rate performance, i.e., 101.8 $mAh\cdot g^{-1}$ at 10C, which hold 72% of the initial capacity at 0.1 C, as shown in Fig.9b.

Without employing templates, hydrothermal synthesis (HTS) as a low-temperatured liquid phase thermal (LPT) synthesis has also been employed to prepare 3D porous $LiFePO_4$ microspheres. In the HTS process, the $LiFePO_4$ precursor nanoparticles precursor particles deposit on account of their small solubility in the solution. Then, the nano-sized $LiFePO_4$ precursor particles self-assemble to form densely packed microspheres necessary for reducing the surface tension of the dispersed particles. Subsequently, with a dissolution-deposition process, the agglomerated $LiFePO_4$ precursors evolve into 3D porous microspheres.[133] The HTS performs lots of advantages such as simplicity, morphology control, homogeneous particle size distribution, and low cost.[134],[135] In 2010, Gao's group[133] first prepared 3D porous $LiFePO_4$ microspheres consisting of nanoparticles by the hydrothermal process. These $LiFePO_4$/C microspheres exhibited high Brunauer-Emmett-Teller (BET) surface areas of 38.6 $m^2\cdot g^{-1}$ and delivered excellent high rate capability of 115 $mAh\cdot g^{-1}$ at 10C. Even at 20C and 30C, they performed 93 $mAh\cdot g^{-1}$ and 71 $mAh\cdot g^{-1}$ respectively. In 2011, Goodenough's group[92] successfully accomplished the self-assembly of $LiFePO_4$ nanoplates for the porous microspheres using STS route, as shown in Fig.8e. It can be seen that the 3D porous $LiFePO_4$/C microspheres (1-3 μm) consist of nanoplates (80 nm), which interweave together forming a flowerlike structure giving a high BET surface area of 32.9 $m^2\cdot g^{-1}$. The as-obtained flowerlike $LiFePO_4$/C microspheres exhibited discharge capacity of 72 $mAh\cdot g^{-1}$ at 10C. Due to the conductive ploymer PPy prossessing macromolecule sp^2-type carbon, The $LiFePO_4$/(C+PPy) performed excellent rate performance, e.g., high discharge capacity of 92 $mAh\cdot g^{-1}$ at 10C. Additionally, Eom's group and Kwon's group[136] provided a growth technology to synthesize porous and coarse $LiFePO_4$/C composites (5-10 μm) using $LiFePO_4$ nanoparticles (100-200 nm) as seed crystals for the 2nd crystallization process, as shown in Fig.8d. The SEM and TEM images of $LiFePO_4$/C composites were shown in Fig.8d. The as-obtained 3D porous $LiFePO_4$/C composites deliverd discharge capacity of 100 $mAh\cdot g^{-1}$ at 10C, which is 65 % of the discharge capacity at 0.1 C. All the excellent rate performance strongly fulfill the requirements of rechargeable lithium batteries for high power applications.

It is worth noting that a versatile spray drying methodology is usually employed to prepare 3D porous spheres with micro-nano-superstructures.[137] Zhang's group[138] reported a novel and simple template-free concept and synthesis of 3D porous $LiFePO_4$/C microspheres via a sol-gel-spray drying (sol-gel-SD) method. As shown in Fig.8f-8i, it is clearly can be seen that the as-obtained $LiFePO_4$/C had a large specific surface area of 20.2 $m^2\cdot g^{-1}$, an average nano-size of 32 nm and a main pore diameter of 45 nm. The as-obtained 3D porous $LiFePO_4$/C microspheres easily contact with electrolyte, which facilitated the Li-ion diffusion, gave a high coulombic efficiency of 97.2%, and presented an excellent capacity retention rate close to 100% after 50 cycles. However, it only gave 100 $mAh\cdot g^{-1}$ at the high rate of 10C, due to less carbon coating and low porosity.[139] When using citric acid as carbon source, 3D porous $LiFePO_4$/C microspheres have been successfully synthesized.[140],[141] Polyvinyl alcohol (PVA) gel has been also chosen as carbon source for its excellent film-forming properties in spray drying process.[142] The carbon layers transformed from carbon sources were well coated around $LiFePO_4$ and showed excellent cyclability and superior rate capability.

3.2 Low temperature performance

$LiFePO_4$ cathode with excellent power output makes it a superior candidate for HEV and EV applications. However, one key challenge is the poor low temperature performances due to $LiFePO_4$ itself and the electrolyte in $LiFePO_4$-based batteries, as compared to the performances at room temperature. In 2013,

Shin's group[143] found that pristine $LiFePO_4$ exhibited a higher cycling stability at lower operating temperature of -20 °C than room temperature. It is suggested that $LiFePO_4$ process the much milder degradation of the surface and the bulk at low temperature. To date, $LiFePO_4$ itself and the electrolyte have been both responsible for the poor low-temperature performance, which is the key challenge for the wide application of $LiFePO_4$ in EES devices.[144]

Generally, carbon coating is used to improve the electron conductivity of the electrodes. The processes are associated with electron conductions.[27],[145] A good electronic conductivity is of crucial importance to facilitate electron conduction and achieve high performances.[146],[147] Carbon is a common low-cost material with good conductivity and is widely used for conductivity improvement. Carbon layers can be facilely coated on the nanostructure surfaces by many low-cost and scalable methods, such as organic chemical polymer coating and annealing.[148] Carbon coating is quite successful in improving the cathode conductivity, but the weight ratio of carbon has to be carefully controlled.[149],[150] To be extreme, a cathode made of pure carbon will simply turn the battery into a double-layer supercapacitor, which has very low energy density and unstable output voltage. Higher carbon content also results in lower volumetric energy density due to the smaller mass density of carbon. Apart from the enhancement of conductivity, carbon also serves as capping material that can effectively reduce the particle growth during crystallization processes. Simultaneously, the reducing atmosphere of carbon also prevents the oxidation of Fe(II) during high temperature annealing.

In 2011, Tu's group[151] successfully prepared carbon-coated $LiFePO_4$ materials using polystyrene (PS) spheres (50-300 nm) as carbon source. The results illustrated that the $LiFePO_4$/C with 3.0 wt% carbon content performed excellent electrochemical capability at low temperature of -20 °C, which delivered 147 $mAh\cdot g^{-1}$ and 79.3 $mAh\cdot g^{-1}$ at 0.1C and 1C respectively (Fig.10). Even after 100 cycles at 1C, the $LiFePO_4$/C still exhibited almost 100% capacity retention. It can be attributed to the optimal carbon coating thickness (2.5 nm) and good carbon coating morphology. Using citric acid as a carbon source, Wang's group[152] reported a kind of 3D $LiFePO_4$/C microspheres. The electronic conductivity of $LiFePO_4$/C microspheres is between 7.5×10^{-2} and 10^{-1} $S\cdot cm^{-1}$ from -40 °C to 23 °C, which gave attractive low temperature discharge capacity of 110 $mAh\cdot g^{-1}$ and 64 $mAh\cdot g^{-1}$ at -20 °C and -40 °C. Alternatively, Scrosati's group and Sun's group[153] provided double-carbon-coated $LiFePO_4$/C porous microspheres, with a excellent specific discharge capacity of 70 $mAh\cdot g^{-1}$ (1C) at -20 °C. Additionally, polyacene (PAS) was also employed to optimize $LiFePO_4$.[154] The as-obtained $LiFePO_4$/PAS microspheres performed outstanding discharge capacity of 88 $mAh\cdot g^{-1}$ at 1C at the lowtemperature of -20 °C. This favorable electrochemical performance is attributed to the homogeneous morphology, the small particles inside, the porous surface, and the conductive PAS (8.5 wt.%).

Besides coating conductive carbon, metal ion doping is another common method to improve the conductivity of the $LiFePO_4$. Various metal dopants have been studied, such as Mg^{2+}, Al^{3+}, Cr^{3+}, Ti^{4+}, Zr^{4+}, Nb^{5+}, W^{6+}, etc. Metal dopant will replace the Li^+ (M1 doping) or Fe^{2+} (M2 doping) in $LiFePO_4$ lattice to generate *n*-type semiconductor. [37] The conductivity can be enhanced by over seven orders of magnitude after doping. It was believed that the dopants replaced metal ions in $LiFePO_4$ lattice, could enhance the electronic and ionic conductivity.[24] In 2011, Liao's group[155] optimized $LiFePO_4$ by slight Mn-substitution. The as-obtained $LiFe_{0.98}Mn_{0.02}PO_4$/C delivered 99.8 $mAh\cdot g^{-1}$ (1C) at -20 °C, which is superior to 90.7 $mAh\cdot g^{-1}$ for $LiFePO_4$/C. Even at the low temperature of -40 °C, the $LiFe_{0.98}Mn_{0.02}PO_4$/C still gave 70.5 $mAh\cdot g^{-1}$ at 1C.

Recently, mixtures of $LiFePO_4$ and $Li_3V_2(PO_4)_3$ (i.e., $xLiFePO_4+yLi_3V_2(PO_4)_3$, $x > 0$, $y > 0$) exhibited excellent electrochemical performance and have recently attracted much attention.[156],[157] Chen's group[144] found that $LiFePO_4$/C delivered only discharge capacity of 45.4 $mAh\cdot g^{-1}$ (0.3C) at −20 °C, being 31.5% of the capacity obtained at 23 °C. Compared with $LiFePO_4$/C, the $Li_3V_2(PO_4)_3$/C could give discharge capacity of 108.1 $mAh\cdot g^{-1}$ (0.3C) at -20 °C, which 86.7% of the capacity at 23 °C. It is found that the activation energies of $LiFePO_4$ and $Li_3V_2(PO_4)_3$ are calculated to be 47.48 $kJ\cdot mol^{-1}$ and 6.57 $kJ\cdot mol^{-1}$, respectively. The Li-ion transform in $Li_3V_2(PO_4)_3$ is much easier than in $LiFePO_4$. Recently, many mixtures of $LiFePO_4$ and $Li_3V_2(PO_4)_3$ have been studied and given excellent rate performance, such as 100 $mAh\cdot g^{-1}$ at 10 C for $2LiFePO_4/C+Li_3V_2(PO_4)_3/C$,[158] 116.8 $mAh\cdot g^{-1}$ at 10 C for $3LiFePO_4/C+Li_3V_2(PO_4)_3/C$,[159] 114 $mAh\cdot g^{-1}$ at 10 C for $5LiFePO_4+Li_3V_2(PO_4)_3$,[160] 93.3 $mAh\cdot g^{-1}$ at 10 C for $9LiFePO_4/C+Li_3V_2(PO_4)_3/C$.[161] However, up to now, the low temperature performance has still been rarely reported. It is worthwhile to examine the influence of the combination of $LiFePO_4$ and $Li_3V_2(PO_4)_3$ on the performance of Li-ion battery, and the low temperature of $LiFe_xV_{2/3-2x/3}PO_4$/C ($0<x<1$) solid state materials.

Electrolyte is another main reason in addition to $LiFePO_4$ itself. The main reason might be the poor performances of conventional $LiPF_6$/EC+DMC+EMC electrolyte system at low temperature. The electrolyte becomes more viscous at low temperature, resulting in a low diffusion coefficient of lithium ions in the electrolyte. Performance degradation can be expected since fast Li-ion diffusion (i.e., shorter intercalation time and better utilization of the active material) is of crucial importance for high performance cathodes. The inherent properties of olivine $LiFePO_4$ might also contribute to the degradations but it is less likely to be the main reason. In the near future, more efforts are need to improve the low temperature performances. Huang's group[35] reported that $LiPF_6$ salt in EC (the high feezing point of 36.4 °C) easily lead to poor Li-ion diffusion at low temperature, particularly below -20 °C. Thus, exploration of novel electrolyte systems with superior low temperature properties might be a promising research direction. The viscosity increase of the electrolyte at low temperature may be the reason.[27] Ma's group[162] provided 1.0 M LiPF6/EC+DMC+DEC+EMC (1:1:1:3, v/v) electrolyte. $LiFePO_4$/C composite could perform 90 $mAh\cdot g^{-1}$ and 69 $mAh\cdot g^{-1}$ at -20 °C and -40 °C respectively. Moreover, Zhang's group[163] found that $LiFePO_4$/C composite could operate over a wide temperature range (-50 to 80 °C) using new lithium salts $LiBF_4$-LiBOB in a solvent mixture of PC+EC+EMC (1:1:3). Although LiBOB-based electrolyte has high conductivity above -10 °C and high temperature performance even up to 90 °C, but it

fails to perform below -40 °C. Fortunately, the mixture of $LiBF_4$ and LiBOB help the electrolyte process a large working temperature range from -50 °C to 90 °C due to high conductivity of $LiBF_4$ below -10 °C. With the help of $LiBF_4$-LiBOB-based electrolyte, LiFePO4 delivered 62 mAh·g^{-1} and 43 mAh·g^{-1} even at -40 °C and -50 °C.

3.3 Volumetric energy density

High volumetric energy density of batteries can make the batteries smaller in volume while exhibiting the same performances.[35],[149] Compared with mass density (5.1 g·cm^{-3}) of the dominant $LiCoO_2$ cathode materials, the theoretical density of $LiFePO_4$ is only 3.6 g·cm^{-3}.[164] However, the tap density of $LiFePO_4$ usually lies in the range of 0.8-1.5 g·cm^{-3}, which seriously limits the volumetric energy density and becomes one main obstacle preventing $LiFePO_4$ to scale commercial application.[35],[165] Optimizing particle morphology and distribution has proven to be helpful for superior performance. Absolutely, spherical architecture of $LiFePO_4$ is preferred to optimize the tap density. Compared with irregular particles, spherical $LiFePO_4$ particles can decrease vacant space between the particles and improve fluidity of the particles. Furthermore, less binder (polyvinylidene fluoride (PVDF) or PTFE) can be stuck to spherical $LiFePO_4$ particles in fabricating the cathode film, which can enhance the volumetric energy density. In addition, the coating carbon with a density of 2.2 g·cm^{-3} consumes the volumetric energy density while enhancing gravimetric energy density efficiently.[27] Thus, it is imperative to consider the weight ratio and optimized the balance to get a high gravimetric energy density without sacrificing the volume energy density for LIBs.

Recently, coprecipitation method,[166] molten-salt method,[167] HTS method,[168] and microwave assisted water-bath reaction (MW-WBR)[169] have been employed to prepare $LiFePO_4$ with high tap density, as shown in Table 2. Coprecipitation method (including controlled crystallization method) is considered as one of the most versatile technique to produce spherical $LiFePO_4$ particles. Firstly, spherical amorphous $FePO_4{\cdot}xH_2O$ powders are prepared by coprecipitation method. Ying's group[166] adopted a reactor (Fig.11a) to prepare microspherical amorphous $FePO_4{\cdot}xH_2O$ powders (Fig.11b) with 8 μm by controlled crystallization method following the reaction: $Fe(NO_3)_3 + H_3PO_4 + 3NH_3 + xH_2O = FePO_4{\cdot}xH_2O + 3NH_4NO_3$. It was found that the pH value should be fixed on 2.1, avoiding the hydrolyzation of PO_4^{3-} into HPO_4^{2-} and $H_2PO_4^-$ as the solution's pH decreases, and protecting the Fe^{3+} from hydrolyzing to $Fe(OH)_2^+$, $Fe(OH)_2^+$ and $Fe(OH)_3$ when the solution's pH increases. Secondly, the Li source, carbon source and some doping element were added with $FePO_4{\cdot}xH_2O$ and then heat treated at the high temperature. Ying's group[166] synthesized spherical $Li_{0.97}Cr_{0.01}FePO_4$/C (Fig.11c) with a tap density of 1.8 g/cm^3, which is superior to 1.37 g·cm^{-3} prepared by ball milling.[170],[171] and similar to 1.82 g·cm^{-3} synthesized by secondary ball milling method.[172] The $Li_{0.97}Cr_{0.01}FePO_4$/C composite exhibited 163 mAh·g^{-1} at 0.005C, but had low discharge capacity 142 mAh·g^{-1} at 0.1C and unsatisfactory rate capability 110 mAh·g^{-1} at 1C (Fig.12a), with corresponding volumetric discharge capacity of 198 mAh·cm^{-3} (Fig.12b). This is due to large amounts of inert $Li_{0.97}Cr_{0.01}FePO_4$ at the heart of the solid $Li_{0.97}Cr_{0.01}FePO_4$ microsphere, which contacted poorly with electrolytes, as shown in Fig.8a.[138]

In order to get a high gravimetric energy density and tap density simultaneously, conductive polymer PAS was employed to improve the rate capability of $LiFePO_4$ using controlled crystallization method.[154] They prepared $LiFePO_4$/PAS with a tap density of 1.6 g·cm^{-3}, which exhibited rate capability of 129 mAh·g^{-1} and 97 mAh·g^{-1} at 1C and 5C respectively, corresponding to volumetric discharge capacity of 206.4 mAh·cm^{-3} and 155.2 mAh·cm^{-3} at 1C and 5C respectively. In 2010, Sun's group and co-workers[173] prepared spherical $LiFePO_4$/C using polyvinylpyrrolidone (PVP) as a carbon source with particle size of 6μm and high tap density of 1.6 g·cm^{-3}. The as-obtained $LiFePO_4$/C performed discharge capability of 132 mAh·g^{-1} (211.2 mAh·cm^{-3}) and 108 mAh·g^{-1} (172.8 mAh·cm^{-3}) at 1C and 5C respectively. Zhang's group[174] improved carbon content of $LiFePO_4$/C to 7.0 wt.% and synthesized the $LiFePO_4$/C with the high tap densigy of 1.8 g·cm^{-3} by coprecipitation method using self-produced high-density $FePO_4$ pressure-filtrated at 20 MPa (Fig.11e). Due to the denser structure, the $LiFePO_4$/C delivered volumetric discharge capability of 300.6 mAh·cm^{-3} at 0.1C. Even at 1C and 5C, the $LiFePO_4$/C also exhibited high capacities of 257.4 mAh·cm^{-3} and 176.9 mAh·cm^{-3}, respectively.

To further improve the high rate performance, 3D porous spongelike $LiFePO_4$/C particles with high tap density of 1.5 g/cm^3 were successfully prepared by the coprecipitation method using pitch as carbon source (Fig.11d).[175] Although each spongelike $LiFePO_4$/C particle with micron size of 6μm consisted of nanoscale 200-300 nm primary $LiFePO_4$/C particles, the spongelike $LiFePO_4$/C particle gave volumetric discharge capacity of 214.5 mAh·cm^{-3} and 186.0 mAh·cm^{-3} at 1C and 5C respectively, which is 2.5 times than that of nano-sized $LiFePO_4$/C with the tap density of 0.6 g·cm^{-3}. In 2010, double carbon coating (sucrose and pitch as carbon source) was employed to synthesized $LiFePO_4$/C, which processed a tap density of 1.5 g·cm^{-3} and gave volumetric discharge capacity of 225.0 mAh·cm^{-3} and 193.5 mAh·cm^{-3} at 1C and 5C.[153] Even at 10C and 20C, the $LiFePO_4$/C delivered 116 mAh·g^{-1} (174.0 mAh·cm^{-3}) and 79 mAh·g^{-1} (118.5 mAh·cm^{-3}), respectively.

In addition to coprecipitation method, Zhou' group[167] prepared microspherical $LiFePO_4$ with a tap density of 1.55 g·cm^{-3} via a molten-salt method, which showed accelerated reaction rate and controllable particle morphology. However, the $LiFePO_4$ product delivered low capacity of 130.3 mAh·g^{-1} (201.5 mAh·cm^{-3}) at 0.1C due to the large amounts of inert $LiFePO_4$ at the heart of the solid $LiFePO_4$ microsphere.[138] In 2011, quasi-microspheres of $LiFePO_4$/C composed of many densely compact nanoplates (with 100 nm size and 30 nm thickness) were synthesized by Zhang's group (Fig.11f).[168] Due to the $FePO_4{\cdot}2H_2O$ nanoplates assembled quasi-microspherical precursors via hydrothermal process, the as-obtained $LiFePO_4$/C quasi-microspheres possessed a tap density of 1.4 g·cm^{-3} and showed excellent high rate performance. Even at 30C current rate, the discharge capacities can reach 75 mAh·g^{-1} (105 mAh·cm^{-3}). In 2014, Kim's group[176] successfully prepared 3D porous $LiFePO_4$ microspheres with a high tap density of (1.7 g·cm^{-3}) using a spray drying (SD) method. The as-obtained 3D porous $LiFePO_4$ microspheres with the carbon content of 3.3%

delivered a high initial discharge capacity of 160 mAh·g^{-1} (272 mAh·cm^{-3}) at 0.1C, corresponding to 94% of the theoretical capacity, as shown in Fig.12.

Interestingly, MW-WBR method was employed to synthesize spherical $LiFePO_4$/C with quite a high tap density of 2.0 g·cm^{-3}, which will strongly benefit the enhancement of volumetric energy density (Fig.11g).[169] This spherical $LiFePO_4$/C exhibited high tap density superior to 1.0 g·cm^{-3} (Tianjin Sterlan-Energy Ltd. China), 1.4 g·cm^{-3} (Phostech lithium Inc., Canada), and 1.5 g·cm^{-3} (Valence Technology Inc.,US).[174] Furthemore, the spherical $LiFePO_4$/C performed excellent discharge capacity of 131 mAh·g^{-1} (262.0 mAh·cm^{-3}) and 105 mAh·g^{-1} (210 mAh·cm^{-3}) at 1C and 5C, respectively.

4 Synthetic reaction mechanism

4.1 Carbothermal reduction method

Recent synthesis approaches and equipments towards cathode material $LiFePO_4$, such as solid phase thermal (SPT) routes and liquid phase thermal (LPT) routes.[177],[178] It is well known that carbothermal reduction (CTR) method is one of the promising SPT methods. CTR method is considered as an effective approach to improving electrochemical performance of $LiFePO_4$ materials.[127],[179] CTR method not only gives special environment favorable for the reduction of Fe(III) and the formation of the $LiFePO_4$/C material, but also provides the continuous conductive carbon film as electron conductor enhancing the electronic conductivity of $LiFePO_4$.[94] Moreover, the evenly distributed carbon can also prevent particle coalescence. Recently, CTR method has been defined as a feasible, low-cost and environmental-friendly method for fabrication of $LiFePO_4$/C composites and has been largely employed to synthesize high performance $LiFePO_4$/C composites.

There are mainly two steps in CTR method. At the first step, carbon sources are evenly distributed in precursor aggregation using various routes, such as ball milling,[180],[181] sol-gel,[182],[183] co-precipitation,[184],[185] , spray drying,[138],[186] *etc*. Carbon sources include inorganic carbon (e.g., carbon black + surface activator), organic sucrose, small molecular acid (e.g., citric acid), big molecular polymer (e.g., PEG10000)[187] and sp2-tapyed carbon (e.g., carbon nanotube (CNT) and graphene).[188],[189] At the second step, $LiFePO_4$/C is formed due to vigorous gas evolution (mainly CO and CO_2) during degradation and carbonization of the carbon sources. During heat treatment of appropriate precursor, elementary carbon is deposited on the walls of primary nanoparticles as a degradation product. Meanwhile, the continuous conductive carbon film can overcome the electronic and lithium-diffusion limitations, improve the rate of insertion/extraction and optimize the electrochemical performance under high-current regimes.

Noticeably, electrochemical performance of $LiFePO_4$/C material is influenced by various carbon sources and raw materials. Iron phosphides, such as FeP and Fe_2P, were reported to have effects on the improvement of the rate performance. Obviously, the impurities especially for Fe_2P easily appeared as by-products in the CTR synthetic process. It is difficult to control the content of Fe_2P, which has effects on the electrochemical performance of $LiFePO_4$. Why Fe_2P was synthesized by carbothermal reaction at different temperature? What is noteworthy is that the phase of Fe_2P could take place in the following conditions, such as self-deoxidization reaction of $LiFePO_4$/C composite, reducing agent iron nanoparticles, stoichiometric excess of Fe_2O_3. Moreover, the Fe_2P could also appear when using microwave assisted CTR (MW-CTR) method. In this part, we focus on synthetic reaction mechanism in CTR synthetic conditions.

4.1.1 Effects of Fe(II) and Fe(III) raw material sources

Usually, Fe(III) sources including $FePO_4$, Fe_2O_3, $Fe(NO_3)_3$ and $Fe(NH_4)_2(SO_4)_2\cdot 6H_2O$ are employed to prepare $LiFePO_4$ via the CTR routes.[190] In our previous research,[94] it is found that $LiFePO_4$/C can be strongly formed at around 450 ^oC by in-situ CTR method whether using various carbon sources except for inorganic carbon sources (postponed to 539 ^oC due to the preparation of $Li_3Fe_2(PO_4)_3$, as shown in Fig.13a and 13b), similar to the reports by Garbarczyk's group[191] and Jiao's Group[192]. Self-deoxidation reaction of $LiFePO_4$/C takes place at 840 ^oC (Table 3), which was in accordance with the results of Wang's group.[193] The crystallization of Fe_2P and $Li_4P_2O_7$ happens at 930 ^oC suggesting that severe decomposition of $LiFePO_4$/C. Normally, in-situ CTR synthetic temperature should be carefully controlled below 840 ^oC to avoid the Fe_2P by-product during the sintering process. However, it was found that suitable content of Fe_2P would improve the electrochemical performance of $LiFePO_4$. Kim's group[194],[195] and Lee's group[196] found that the Fe_2P content increased with increasing carbon content at the temperature of 900 ^oC, as shown in Fig.13c. As the carbon content was above 12 wt%, a large amount of $LiFePO_4$/C disappeared and Fe_2P was predominantly produced.

Besides Fe(III) raw material source, FeC_2O_4 was generally employed as Fe(II) raw material source to synthesize $LiFePO_4$. It can be seen that the presence of Fe_2P appeared at 675 ^oC.[197],[198] Zboril's group[199] and Molenda's group[200] found that reducing agents including α-Fe nanoparticles, magnetic Fe_3O_4 and Fe_3C could be obtained during the thermal decomposition of $FeC_2O_4\cdot 2H_2O$ in a dry argon flow. These reducing agents especially for Fe particles could react with $LiFePO_4$/C and generate Fe_2P around 700 ^oC.[201],[202] It was worth noting that iron phosphides increased with the increase of excessively stoichiometric iron source and the temperature.[203],[204]

4.1.2 Reductive atmosphere of hydrogen

In addition to self-deoxidization reaction of $LiFePO_4$/C composite and reducing agents from Fe raw materials sources, reductive atmosphere of hydrogen also reduced $LiFePO_4$ to prepare Fe_2P at 600 ^oC according to the work of Nazar's group.[99] The Fe_2P can be observed after the sintering process at 600 ^oC for 4 h in gas atmosphere of N_2/H_2=97/3 (vol.%) reported by Taniguchi's group.[205],[206] Furthermore, the phase of FeP and Fe_3P could also be observed.[207] Wohlfahrt-Mehrens's group[208] studied various gas atmospheres and considered that some traces of Fe(III) could be confirmed when using Fe(II) raw sources but not enough reductive additive (e.g. N_2/H_2=99/1 (vol.%), no carbon as reductive additive). According to the results, the authors suggested that a considerable amount of Fe_2P was generated as the hydrogen raised to 10 vol.%, as shown in

Fig.13d. The amount of Fe_2P would increase with the carbon addition. Additionally, it is important to note that $LiFePO_4$ will decompose into Fe_2P, Li_3PO_4, $Li_4P_2O_7$ and Li_3P_7 when the heating temperature reaches 850 ^oC under a stream of a gas mixture of Ar/H_2=95/5 (vol.%).[209]

4.1.3 Microwave assisted carbothermal reduction method

Compared with conventional CTR method, MW-CTR method has recently attracted much attention.[177] Microwave irradiation (2.54 GHz) can provide "inert and instant heating", and exhibit outstanding superiority such as fast response, time effectiveness, low energy consumption, and environmentally benighity.[210],[211] Moreover, microwave irradiation was also adopted to optimize the physical and electrochemical performance of $LiFePO_4$.[212] Under Ar atmosphere, Higuchi's group[213] found that iron acetate acts as a microwave susceptor rather than iron lactate. The result illustrate that $LiFePO_4$ was successfully prepared using iron acetate as Fe sources at 500 W for 10min, whereas $LiFePO_4$ was not observed using iron lactate as Fe raw sources even up to 30min. Furthermore, the microwave irradiation time has important effect on the Fe_2P by-products, which could increase with the increasing time due to the work of Kwon's group[214] All the phases of $LiFePO_4$, Fe_2P and $Li_4P_2O_7$ were observed when the amount of Fe_2P is above 1.0 wt.%.[215] In addition to Ar atmosphere, carbon materials and carbon sources were both employed to produce vigorous CO gas, which is curious for the preparation of $LiFePO_4$.[216],[217] Thanks to this strategy, the electrochemical performance of $LiFePO_4$ was strongly improved by MW-CRT method using carbon coating,[218] multi-walled CNTs (MWCNTs) doping,[219] Mo and La doping.[220],[221] However, it is worthwhile to note that most of the carbon could be consumed after extended heating treatment. The transformation from Fe(II) to Fe(III) would take place, leading to impurity phases of Fe_2O_3 and $Li_3Fe_2(PO_4)_3$.[222],[223] Therefore, the microwave-derived and phase-pure $LiFePO_4$ without impurities could be successfully synthesized via MW-CTR method under the certain proper conditions.

4.2 Low-temperatured liquid phase thermal synthesis

In addition to high-temperatured CTR method, the low-temperatured LPT routes, such as HTS, STS and ionothermal synthesis (ITS), provided more effective pathways to synthesize $LiFePO_4$. HTS and STS are generally LPT synthetic methods, which exhibit lots of advantages including morphology control, homogeneous particle size distribution, relatively low temperature (≤300 ^oC), low cost and simplicity.[224],[225] Recently, HTS and STS are both largely employed to prepare special morphologic $LiFePO_4$, such as crystalline growth, nano-structured $LiFePO_4$ and 3D porous $LiFePO_4$ architectures with micro-nano-structures (see section 3.1.1 in this article).[127],[226] In order to improve traditional intermittent reactors for HTS and STS, Teja's group[227] and Aimable's group[228] designed the continuous hydrothermal synthesis, which poise great promise in practical industrial applications. Different form HTS (using water as the main mineralizer) and STS (using organic solvents as main mineralizers), room temperature ionic liquids (RTILs) are regarded as a novel class of mineralizer, which have been employed in ITS route to synthesize cathode materials especially $LiFePO_4$ with nano-structures.[229],[230],[231] Moreover, microwave irradiation is expected to assist HTS, STS and ITS, due to energy- and time-saving advantages of microwave. In this part, we focus on the effects of stoichiometric ratio of raw sources, pH values of solution, additive mediations (e.g., organic acids, surfactants and solvents), and microwave irradiation.

4.2.1 Stoichiometric ratio of raw sources

Usually, the crystalline powders of $LiFePO_4$ were synthesized by mixing amounts of the reactants LiOH, $FeSO_4$ and H_3PO_4 in the stoichiometric ratio of $n_{Li}:n_{Fe}:n_P$ = 3:1:1, as shown in Table 4.[232] Advisable addition of LiOH should be changed with replacing the H^+ with NH_4^+ in H_3PO_4. Kanamura's group[233],[234] found that the stoichiometric ratio of 2.5:1:1 would be better when using $(NH_4)_3PO_4$ instead of H_3PO_4. The stoichiometric ratio of 1:1:1 and 2:1:1 were both appropriate for using $(NH_4)_2HPO_4$. As shown in Fig.14, Our group investigated the products when using $NH_4H_2PO_4$ as PO_4^{3-} source. It can be seen that a large amount of $Fe_3(PO_4)_2{\cdot}H_2O$ as impurity was obtained in the case of x=1.0. As the x value changed into 1.5, more crystalline of $LiFePO_4$ was observed. The value of x=2.0 is obviously in favor of hydrothermal crystallization of pure $LiFePO_4$. The overmuch addition of LiOH (e.g., x=2.5 and 3.0) caused the impurity of Li_3PO_4. All the results strongly suggested that the addition of LiOH should be changed as the PO_4^{3-} source was changed. However, the stoichiometric ratio should be changed back to 3:1:1 when the other Li sources including LiCl and CH_3COOLi were used instead of LiOH.[235],[236] It is noteworthy that $LiFePO_4$ with pure phase was also prepared by using other Fe(II) slats such as $FeCl_2$ and $(NH_4)_2Fe(SO_4)_2$ instead of $FeSO_4$, but the stoichiometric ratio remained unchanged.[237],[238] Furthermore, the $LiFePO_4$ was also successfully synthesized using fresh $Fe_3(PO_4)_2{\cdot}5H_2O$ and Li_3PO_4.[239]

Additionally, Whittingham's group[240] suggested that the $LiFePO_4$ should only be obtained at neutral and slightly basic conditions. Fe disorder onto the Li sites (ca. 3.5%) generally happened at pH value of 6.30. Even the synthetic condition temperature below 175 ^oC, there would be some amounts of Fe on Li sites.[241],[242] Moreover, the synthetic time also had effects on the $LiFePO_4$ nanocrystalline. In 2013, Ou's group[243] found that the peak intensities of (020) X-ray diffraction line of $LiFePO_4$ nanoplates increased with the reaction time prolonging from 0 to 6 h. Meanwhile the relative peak intensities of (020) to (111) also increased, due to the result calculated from XRD patterns of $LiFePO_4$ nanoplates. All the results demonstrated that the $LiFePO_4$ nanoplates have a preferred crystal orientation with large (010) face, which is in favor of good electrochemical performance for $LiFePO_4$.[244]

4.2.2 Additive mediations of organic acids, surfactants and solvents

In addition to the synthetic temperature, residence time, reactant concentration and pH value,[245] additive mediations including organic acids, surfactants and solvents also have effects on the purity, morphology control and electrochemical performance of $LiFePO_4$.[246] Firstly, organic acid not only effects

pH value, but also can be used as reduction mediator. Whittingham's group[247] provided that both of the reduction from Fe(III) into Fe(II) and the formation of the desired $LiFePO_4$ compound carried out with the addition of L-ascorbic acid. Moreover, it was found that the pH value and reaction time played multifold roles in self-assembled mesoporous $LiFePO_4$ with hierarchical spindle-like architectures.[248] When the value of pH increased from 7.0 to 10.0, primary nanocrystals disappeared and spindle-like hierarchical $LiFePO_4$ particles formed. The full transformation from Li_3PO_4 to $LiFePO_4$ nanocrystal needs a reation time over 5 h. Furthermore, in the presence of organic acid, e.g. citric acid or ascorbic acid, well-crystallized $LiFePO_4$ nanoparticles have been directly synthesized.[249] Chung's group and Grey's group[250] successfully controlled the morphological transformations of $LiFePO_4$ particles during the hydrothermal reaction in the presence of citric acid and ammonium ions (NH^{4+}).

Secondly, organic surfactants or polymers including O,O-Bis(2-aminopropyl)polypropyleneglycol (D230), EO20PO70EO20(P123), cyltrimethylammonium bromide(CTAB), sodium dodecyl sulfate(SDS), poly(ethylene glycol) (PEG), *etc*., have been successfully employed to control the particle growth and size distribution. The results from Nazar's group[106] showed the particle size of $LiFePO_4$ became smaller and much more homogeneous compared to that of products using molecular reducing agents, if non-ionic surfactants, including pluronic P123 and Jeffamine D230 were added to the reactors. These years, Gerbaldi and his co-workers[251],[252],[253] investigated the effects of organic surfactant compound CTAB on $LiFePO_4$ characteristics and electrochemical behavior. It is clearly found that CTAB influences deeply during the synthesis and the electrochemical properties of $LiFePO_4$. Moreover, the CTAB micelles are beneficial for controlling the grain size and sucrface area. Additionally, nitrilotriacetic acid (NTA) surfactant has been also employed to synthesize $LiFePO_4$ nanowires.[254] In 2010, Zhang's group[168] used SDS to assist the synthesis of $LiFePO_4$ via hydrothermal process. The as-obtained $LiFePO_4$/C microspheres are composed of primary $LiFePO_4$/C nanoplates with the size of 100 nm and thickness of 30 nm. With the addition of SDS and Ethylenediamine (EN), our group successfully synthesized $LiFePO_4$/C microspheres assembled from nanorods, as shown in Fig.15c and 15d.

Thirdly, hybrids of water and organic solvents have been also employed in the STS route. In 2013, Liao's group[255] successfully prepared high-performance $LiFePO_4$ microspheres consisting of nanofibers (Fig.15a) by a high pressure alcohol-thermal approach in a water and 1,2-propanediol (PD) composite solvent. With the effect of the PD solvent, the $LiFePO_4$ crystalline nuclei were linearly elongated to form into nanofibers. The $LiFePO_4$ nanofibers aggregated together and formed $LiFePO_4$ microspheres. Tetraethylene glycol (TEG) has been also used as consolvent with water.[111] As shown in Fig.15b, rectangular $LiFePO_4$ nanoplatelets were formed with a very thin thickness of 50-80 nm, favouring fast Li-ion diffusion. Moreover, PEG has been usually used to assist morphology control of $LiFePO_4$.[256],[257] Meanwhile, Liu's group[112] provided a water-PEG400 binary solvent to assist solvothermal method and prepare $LiFePO_4$ nanoparticles (50 nm in size), hexagonal nanoplates (800 nm wide and 100 nm thick) and hexagonal microplates (3 mm wide and 300 nm thick).

Recently, RTILs have been also been used as the solvent and template to synthesize $LiFePO_4$. With this new and promising ITS method, Tarascon's group[178],[229] enable $LiFePO_4$ crystalline growth with controlled morphology and size around 250 ^oC. As shown in Fig. 15g-i, large $LiFePO_4$ needles were assembled of Lego blocks. As shown in Fig.15e and 15f, Teng and co-workers[258] successfully prepared $LiFePO_4$ nanorods in an ionic liquid in the presence of sodium dodecyl benzene sulfonate (SDBS) surfactant and ascorbic acid. Thus, super architectures with micro-nano-structured nanocrystals and morphology control with addition of organic acids, organic surfactants and organic solvents.

4.2.3 Microwave-assisted liquid phase thermal routes

Undoubtedly, microwave irradiation has been employed to assist LPT routes, because microwave irradiation assisted synthesis (MIAS) exhibited overwhelming superiorities such as heating the precursor volumely and quickly, efficient and suitable for large-scale synthesis for the practical application of electrode materials. In our prious work,[177] we strongly review the MW-LPT including MW-HTS,[259],[260] MW-STS[261] and MW-ITS.[178] The Li-ion diffusion can be strongly improved by controlling morphology of $LiFePO_4$ via MW-LPT. Moreover, electronic conductivity can be optimized by coating conductive materials such as carbon[262],[263], CNT[264],[265] and conductive polymer, e.g., Poly(3,4-ethylenedioxythiophene)(PEDOT).[266]

5 Conclusion and perspective

In summary, the pathway of Li-ion diffusion in Li_xFePO_4 is mainly along the [010] direction. Sometimes, 2D Li-ion transport carries out along both the [010] and [001] directions at the elevated temperature. Undoubtedly, the phase transformation of $LiFePO_4$ and $FePO_4$ are affected by various conditions, such as particle size, charge/discharge rate, temperature, *etc*. To date, many phase transformation models, including shrinking core (i.e., core–shell) model, Laffont's (i.e., new core-shell) model, mosaic model, domino-cascade model, phase transformation wave model, and many-particle model, have been proposed to explain the lithiation/delithiation process and the phase transformation in Li_xFePO_4. However, these models are still in disagreement with each other. Generally, the two-phase transformation models can be used to explain a two-phase growth process involving the coexistence of $LiFePO_4$ and $FePO_4$ for the large particle, below a critical current and at a relative low temperature. Simultaneously, the quasi-single-phase transformation models are dominantly used in the solid-solution reaction where Li_xFePO_4 particles do not separate into Li-rich and Li-poor phases during lithiation/delithiation process.

In order to endow the $LiFePO_4$ with excellent electrochemical performance including high rate capability, and low temperature performance, reducing the pathway of Li-ion diffusion, particularly [010] direction, is effective route. Usually, fast Li-ion diffusion is achieved by morphology controlling, such as crystal growth orinetation along the a-c plane, nano-sized morphologies and 3D porous architectures with micro-nano-structures. Meanwhile, the electronic conductivity is improved by

coating conductive materials, e.g., amorphous carbon, CNT, graphene, PAS, PPy, Fe_2P, *etc*. However, achieving both high rate performance and volumetric energy density is still a big challenge. Recently, carbon coated $LiFePO_4$ microspheres with a highest tap density of 2.0 $g{\cdot}cm^{-3}$ has been successfully synthesized by MW-WBR method. It can deliver the outstanding discharge capacities of 93 $mAh{\cdot}g^{-1}$ and 78 $mAh{\cdot}g^{-1}$ even at 10 and 20 C respectively. This additional strategy provides a facile and novel route for preparing high tap density of $LiFePO_4$, and holds the potential to be extended for the EES devices.

In addition, it is noteworthy that synthetic reactions play an important role to imporve performance of $LiFePO_4$ cathodes. When using CTR method, the purity of $LiFePO_4$ is significantly affected by the Fe sources, carbon sources and the reductive atmosphere. Obviously, the impurities particularly for Fe_2P are easily by-produced. To date, controlling the content of Fe_2P is still a major obstacle and issue, where the Fe_2P either provides the high conductive networks for $LiFePO_4$ or blocks the pathway of Li-ion diffusion. Low-temperatured LPT synthesis can be also employed to prepare $LiFePO_4$ with much reduced impurities. However, both the crystalline and electrochemical performance of $LiFePO_4$ still need to be enhanced by subsequent heat treatment. Intriguingly, on account of "inert and instant heating", MIAS can be used to assist both CTR route and LPT route. We believe that MIAS provides an extremely fficient and suitable route for large-scale synthesis of $LiFePO_4$ electrode material.

Acknowledgements

The authors highly acknowledge the authors and publications data of the original materials. We would like to thank Dr. Chaoyi Yan, Prof. Haibin Su (School of Materials Science and Engineering, Nanyang Technological University (MSE, NTU)) and Prof. Jianyi Lin (Institute of Chemical and Engineering Sciences, Agency for Science, Technology and Research (ICES, A*STAR)) for their helpful discussions. This work was financially supported by Scientific Research Start-up Fund for High-Level Talents, Shihezi University (No. RCZX201305), the Doctor Foundation of Bingtuan (No. 2014BB004), the Program for Changjiang Scholars and Innovative Research Team in University (No. IRT1161) and the Program of Science and Technology Innovation Team in Bingtuan (No. 2011CC001)

Notes and references

[a] *Key Laboratory for Green Processing of Chemical Engineering of Xinjiang Bingtuan, School of Chemistry and Chemical Engineering, Shihezi University, Shihezi 832003, P.R. China. Email: yufeng05@mail.ipc.ac.cn (F. Yu) and daibin_bce@shzu.edu.cn (B. Dai).*

[b] *Institute of Chemical and Engineering Sciences, Agency for Science, Technology and Research (A*STAR), Jurong Island 627833, Singapore.*

[c] *Key Laboratory of Xinjiang Phytomedicine Resources of Ministry of Education, School of Pharmacy, Shihezi University, Shihezi 832002, P.R. China.*

[d] *Graphene & Energy Storage Technology Research Center, China Energine International (Holdings) Limited, Beijing 100176, P.R. China.*

[e] *Engineering Research Center of Materials-Oriented Chemical Engineering of Xinjiang Production and Construction Corps, Shihezi 832003, P.R. China.*

[f] *Key Laboratory of Materials-Oriented Chemical Engineering of Xinjiang Uygur Autonomous Region, Shihezi 832003, P.R. China.*

[1] K. Mizushima, P. C. Jones, P. J. Wiseman, J. B. Goodenough, *Mater. Res. Bull.* **1980**, *15*, 783-789.
[2] T. Nagaura, K. Tazawa, *Progress in Batteries & Solar Cells* **1990**, *9*, 209-217.
[3] B. Xu, D. N. Qian, Z. Y. Wang, Y. S. L. Meng, *Mat Sci Eng R* **2012**, *73*, 51-65.
[4] M. Wagemaker, F. M. Mulder, *Accounts of Chemical Research* **2013**, *46*, 1206-1215.
[5] J. Cabana, L. Monconduit, D. Larcher, M. R. Palacin, *Adv. Mater.* **2010**, *22*, E170-E192.
[6] X. P. Gao, H. X. Yang, *Energy & Environmental Science* **2010**, *3*, 174-189.
[7] M. R. Palacin, *Chem. Soc. Rev.* **2009**, *38*, 2565-2575.
[8] S. Chu, A. Majumdar, *Nature* **2012**, *488*, 294-303.
[9] J. M. Tarascon, M. Armand, *Nature* **2001**, *414*, 359-367.
[10] R. Marom, S. F. Amalraj, N. Leifer, D. Jacob, D. Aurbach, *J. Mater. Chem.* **2011**, *21*, 9938-9954.
[11] M. Wakihara, *Mat Sci Eng R* **2001**, *33*, 109-134.
[12] A. S. Arico, P. Bruce, B. Scrosati, J. M. Tarascon, W. Van Schalkwijk, *Nature Materials* **2005**, *4*, 366-377.
[13] M. Gong, G. Wall, *Exergy, An International Journal* **2001**, *1*, 217-233.
[14] K. Zaghib, A. Mauger, C. M. Julien, *J. Solid State Electrochem.* **2012**, *16*, 835-845.
[15] J. B. Goodenough, Y. Kim, *Chem. Mater.* **2010**, *22*, 587-603.
[16] M. S. Islam, C. A. J. Fisher, *Chem. Soc. Rev.* **2014**, *43*, 185-204.
[17] M. S. Whittingham, *Chem. Rev.* **2004**, *104*, 4271-4302.
[18] F. Yu, J. J. Zhang, C. Y. Wang, J. Yuan, Y. F. Yang, G. Z. Song, *Progress in Chemistry* **2010**, *22*, 9-18.
[19] Y. Gu, D. Chen, X. Jiao, *The Journal of Physical Chemistry B* **2005**, *109*, 17901-17906.
[20] K. Y. Chung, K. B. Kim, *Electrochimica Acta* **2004**, *49*, 3327-3337.
[21] J. Vetter, P. Novak, M. R. Wagner, C. Veit, K. C. Moller, J. O. Besenhard, M. Winter, M. Wohlfahrt-Mehrens, C. Vogler, A. Hammouche, *J Power Sources* **2005**, *147*, 269-281.
[22] A. K. Padhi, K. S. Nanjundaswamy, C. Masquelier, S. Okada, J. B. Goodenough, *J. Electrochem. Soc.* **1997**, *144*, 1609-1613.
[23] A. K. Padhi, K. S. Nanjundaswamy, J. B. Goodenough, *J. Electrochem. Soc.* **1997**, *144*, 1188-1194.
[24] S. Y. Chung, J. T. Bloking, Y. M. Chiang, *Nature Materials* **2002**, *1*, 123-128.
[25] J. W. Fergus, *J. Power Sources* **2010**, *195*, 939-954.
[26] C. A. J. Fisher, V. M. H. Prieto, M. S. Islam, *Chem. Mater.* **2008**, *20*, 5907-5915.
[27] Y. G. Wang, P. He, H. S. Zhou, *Energy & Environmental Science* **2011**, *4*, 805-817.
[28] M. S. Islam, P. R. Slater, *MRS Bull.* **2009**, *34*, 935-941.
[29] D. D. MacNeil, Z. H. Lu, Z. H. Chen, J. R. Dahn, *J. Power Sources* **2002**, *108*, 8-14.
[30] K. Zaghib, P. Charest, A. Guerfi, J. Shim, M. Perrier, K. Striebel, *J. Power Sources* **2004**, *134*, 124-129.
[31] S. P. Ong, V. L. Chevrier, G. Hautier, A. Jain, C. Moore, S. Kim, X. H. Ma, G. Ceder, *Energy & Environmental Science* **2011**, *4*, 3680-3688.
[32] W. J. Zhang, *J. Power Sources* **2011**, *196*, 2962-2970.
[33] P. P. Prosini, M. Lisi, D. Zane, M. Pasquali, *Solid State Ionics* **2002**, *148*, 45-51.
[34] D. W. Liu, G. Z. Cao, *Energy & Environmental Science* **2010**, *3*, 1218-1237.
[35] L. X. Yuan, Z. H. Wang, W. X. Zhang, X. L. Hu, J. T. Chen, Y. H. Huang, J. B. Goodenough, *Energy & Environmental Science* **2011**, *4*, 269-284.
[36] D. Morgan, A. Van der Ven, G. Ceder, *Electrochem. Solid State Lett.* **2004**, *7*, A30-A32.
[37] M. S. Islam, D. J. Driscoll, C. A. J. Fisher, P. R. Slater, *Chem. Mater.* **2005**, *17*, 5085-5092.

[38] C. Y. Ouyang, S. Q. Shi, Z. X. Wang, X. J. Huang, L. Q. Chen, *Physical Review B* **2004**, *69*, 104303.
[39] X. F. Ouyang, M. L. Lei, S. Q. Shi, C. L. Luo, D. S. Liu, D. Y. Jiang, Z. Q. Ye, M. S. Lei, *J. Alloys Compd.* **2009**, *476*, 462-465.
[40] S. Nishimura, G. Kobayashi, K. Ohoyama, R. Kanno, M. Yashima, A. Yamada, *Nature Materials* **2008**, *7*, 707-711.
[41] J. J. Yang, J. S. Tse, *J. Phys. Chem. A* **2011**, *115*, 13045-13049.
[42] J. B. Goodenough, *J. Power Sources* **2007**, *174*, 996-1000.
[43] M. Park, X. C. Zhang, M. D. Chung, G. B. Less, A. M. Sastry, *J. Power Sources* **2010**, *195*, 7904-7929.
[44] J. Y. Li, W. L. Yao, S. Martin, D. Vaknin, *Solid State Ionics* **2008**, *179*, 2016-2019.
[45] R. Malik, D. Burch, M. Bazant, G. Ceder, *Nano Lett.* **2010**, *10*, 4123-4127.
[46] B. L. Ellis, K. T. Lee, L. F. Nazar, *Chem. Mater.* **2010**, *22*, 691-714.
[47] R. Amin, J. Maier, P. Balaya, D. P. Chen, C. T. Lin, *Solid State Ionics* **2008**, *179*, 1683-1687.
[48] B. Ellis, L. K. Perry, D. H. Ryan, L. F. Nazar, *J. Am. Chem. Soc.* **2006**, *128*, 11416-11422.
[49] G. K. P. Dathar, D. Sheppard, K. J. Stevenson, G. Henkelman, *Chem. Mater.* **2011**, *23*, 4032-4037.
[50] V. Srinivasan, J. Newman, *J. Electrochem. Soc.* **2004**, *151*, A1517-A1529.
[51] L. Laffont, C. Delacourt, P. Gibot, M. Y. Wu, P. Kooyman, C. Masquelier, J. M. Tarascon, *Chem. Mater.* **2006**, *18*, 5520-5529.
[52] A. S. Andersson, B. Kalska, L. Haggstrom, J. O. Thomas, *Solid State Ionics* **2000**, *130*, 41-52.
[53] A. S. Andersson, J. O. Thomas, *J. Power Sources* **2001**, *97-8*, 498-502.
[54] C. Delmas, M. Maccario, L. Croguennec, F. Le Cras, F. Weill, *Nature Materials* **2008**, *7*, 665-671.
[55] R. Dedryvere, M. Maccario, L. Croguennec, F. Le Cras, C. Delmas, D. Gonbeau, *Chemistry of Materials* **2008**, *20*, 7164-7170.
[56] D. Burch, G. Singh, G. Ceder, M. Z. Bazant, in *Theory, Modeling and Numerical Simulation of Multi-Physics Materials Behavior, Vol. 139* (Eds.: V. Tikare, G. E. Murch, F. Soisson, J. K. Kang), **2008**, pp. 95-100.
[57] G. K. Singh, G. Ceder, M. Z. Bazant, *Electrochim. Acta* **2008**, *53*, 7599-7613.
[58] W. Dreyer, J. Jamnik, C. Guhlke, R. Huth, J. Moskon, M. Gaberscek, *Nature Materials* **2010**, *9*, 448-453.
[59] N. Meethong, H. Y. S. Huang, S. A. Speakman, W. C. Carter, Y. M. Chiang, *Adv. Funct. Mater.* **2007**, *17*, 1115-1123.
[60] G. Y. Chen, X. Y. Song, T. J. Richardson, *Electrochem. Solid State Lett.* **2006**, *9*, A295-A298.
[61] P. P. Prosini, *J. Electrochem. Soc.* **2005**, *152*, A1925-A1929.
[62] D. X. Gouveia, V. Lemos, J. A. C. de Paiva, A. G. Souza, J. Mendes, S. M. Lala, L. A. Montoro, J. M. Rosolen, *Physical Review B* **2005**, *72*, 024105.
[63] D. Li, T. Zhang, X. Z. Liu, P. He, R. W. Peng, M. Wang, M. Han, H. S. Zhou, *J. Power Sources* **2013**, *233*, 299-303.
[64] C. V. Ramana, A. Mauger, F. Gendron, C. M. Julien, K. Zaghib, *J. Power Sources* **2009**, *187*, 555-564.
[65] Y. Orikasa, T. Maeda, Y. Koyama, H. Murayama, K. Fukuda, H. Tanida, H. Arai, E. Matsubara, Y. Uchimoto, Z. Ogumi, *Chem. Mater.* **2013**, *25*, 1032-1039.
[66] W. C. Chueh, F. El Gabaly, J. D. Sugar, N. C. Bartelt, A. H. McDaniel, K. R. Fenton, K. R. Zavadil, T. Tyliszczak, W. Lai, K. F. McCarty, *Nano Lett.* **2013**, *13*, 866-872.
[67] P. Bai, G. Y. Tian, *Electrochim. Acta* **2013**, *89*, 644-651.
[68] T. Ichitsubo, K. Tokuda, S. Yagi, M. Kawamori, T. Kawaguchi, T. Doi, M. Oishi, E. Matsubara, *J Mater Chem A* **2013**, *1*, 2567-2577.
[69] S. Dargaville, T. W. Farrell, *Electrochim. Acta* **2013**, *94*, 143-158.
[70] L. Wang, T. Maxisch, G. Ceder, *Physical Review B* **2006**, *73*, 195107.
[71] J. P. Perdew, K. Burke, M. Ernzerhof, *Phys. Rev. Lett.* **1996**, *77*, 3865-3868.
[72] M. S. A. Rasiman, F. W. Badrudin, T. I. T. Kudin, M. K. Yaakob, M. F. M. Taib, M. Z. A. Yahya, O. H. Hassan, *Integr Ferroelectr* **2014**, *155*, 71-79.
[73] S. Leoni, M. Baldoni, L. Craco, J. O. Joswig, G. Seifert, *Z Phys Chem* **2012**, *226*, 95-106.
[74] M. E. A. Y. de Dompablo, N. Biskup, J. M. Gallardo-Amores, E. Moran, H. Ehrenberg, U. Amador, *Chem. Mater.* **2010**, *22*, 994-1001.
[75] S. Q. Yang, T. R. Zhang, Z. L. Tao, J. Chen, *Acta Chim Sinica* **2013**, *71*, 1029-1034.
[76] N. Marx, L. Croguennec, D. Carlier, A. Wattiaux, F. Le Cras, E. Suard, C. Delmas, *Dalton Trans.* **2010**, *39*, 5108-5116.
[77] L. Gu, C. B. Zhu, H. Li, Y. Yu, C. L. Li, S. Tsukimoto, J. Maier, Y. Ikuhara, *Journal of the American Chemical Society* **2011**, *133*, 4661-4663.
[78] R. Malik, F. Zhou, G. Ceder, *Nature Materials* **2011**, *10*, 587-590.
[79] G. Y. Chen, X. Y. Song, T. J. Richardson, *J. Electrochem. Soc.* **2007**, *154*, A627-A632.
[80] P. Bai, D. A. Cogswell, M. Z. Bazant, *Nano Lett.* **2011**, *11*, 4890-4896.
[81] J. L. Dodd, R. Yazami, B. Fultz, *Electrochem. Solid State Lett.* **2006**, *9*, A151-A155.
[82] C. Delacourt, J. Rodriguez-Carvajal, B. Schmitt, J. M. Tarascon, C. Masquelier, *Solid State Sciences* **2005**, *7*, 1506-1516.
[83] C. Delacourt, P. Poizot, J. M. Tarascon, C. Masquelier, *Nature Materials* **2005**, *4*, 254-260.
[84] A. Yamada, H. Koizumi, S. I. Nishimura, N. Sonoyama, R. Kanno, M. Yonemura, T. Nakamura, Y. Kobayashi, *Nature Materials* **2006**, *5*, 357-360.
[85] P. Gibot, M. Casas-Cabanas, L. Laffont, S. Levasseur, P. Carlach, S. Hamelet, J. M. Tarascon, C. Masquelier, *Nature Materials* **2008**, *7*, 741-747.
[86] N. Meethong, H. Y. S. Huang, W. C. Carter, Y. M. Chiang, *Electrochem. Solid State Lett.* **2007**, *10*, A134-A138.
[87] J. Maier, *Nature Materials* **2005**, *4*, 805-815.
[88] X. L. Wu, L. Y. Jiang, F. F. Cao, Y. G. Guo, L. J. Wan, *Adv. Mater.* **2009**, *21*, 2710-2714.
[89] P. G. Bruce, B. Scrosati, J. M. Tarascon, *Angew. Chem.-Int. Edit.* **2008**, *47*, 2930-2946.
[90] Y. Wang, G. Z. Cao, *Adv. Mater.* **2008**, *20*, 2251-2269.
[91] F. Yu, J. J. Zhang, Y. F. Yang, G. Z. Song, *J. Power Sources* **2010**, *195*, 6873-6878.
[92] C. W. Sun, S. Rajasekhara, J. B. Goodenough, F. Zhou, *J. Am. Chem. Soc.* **2011**, *133*, 2132-2135.
[93] G. X. Wang, L. Yang, S. L. Bewlay, Y. Chen, H. K. Liu, J. H. Ahn, *J. Power Sources* **2005**, *146*, 521-524.
[94] F. Yu, J. J. Zhang, Y. F. Yang, G. Z. Song, *Electrochim. Acta* **2009**, *54*, 7389-7395.
[95] Y. Ding, Y. Jiang, F. Xu, J. Yin, H. Ren, Q. Zhuo, Z. Long, P. Zhang, *Electrochem. Commun.* **2010**, *12*, 10-13.
[96] B. Jin, E. M. Jin, K. H. Park, H. B. Gu, *Electrochem. Commun.* **2008**, *10*, 1537-1540.
[97] Z. L. Liu, S. W. Tay, L. A. Hong, J. Y. Lee, *J. Solid State Electrochem.* **2011**, *15*, 205-209.
[98] C. S. Li, S. Y. Zhang, F. Y. Cheng, W. Q. Ji, J. Chen, *Nano Res* **2008**, *1*, 242-248.
[99] Y. H. Rho, L. F. Nazar, L. Perry, D. Ryan, *J. Electrochem. Soc.* **2007**, *154*, A283-A289.
[100] P. S. Herle, B. Ellis, N. Coombs, L. F. Nazar, *Nature Materials* **2004**, *3*, 147-152.
[101] S. X. Zhao, H. Ding, Y. C. Wang, B. H. Li, C. W. Nan, *J. Alloys Compd.* **2013**, *566*, 206-211.
[102] S. Hamelet, M. Casas-Cabanas, L. Dupont, C. Davoisne, J. M. Tarascon, C. Masquelier, *Chem. Mater.* **2011**, *23*, 32-38.
[103] J. Molenda, J. Marzec, *Funct Mater Lett* **2008**, *1*, 97-104.

[104] C. A. J. Fisher, M. S. Islam, *J. Mater. Chem.* **2008**, *18*, 1209-1215.
[105] S. Franger, F. Le Cras, C. Bourbon, H. Rouault, *J. Power Sources* **2003**, *119*, 252-257.
[106] B. Ellis, W. H. Kan, W. R. M. Makahnouk, L. F. Nazar, *J. Mater. Chem.* **2007**, *17*, 3248-3254.
[107] L. Wang, F. Zhou, Y. S. Meng, G. Ceder, *Physical Review B* **2007**, *76*, 165435.
[108] Y. S. Meng, M. E. Arroyo-de Dompablo, *Energy & Environmental Science* **2009**, *2*, 589-609.
[109] C. Y. Nan, J. Lu, L. H. Li, L. L. Li, Q. Peng, Y. D. Li, *Nano Res* **2013**, *6*, 469-477.
[110] J. Lim, V. Mathew, K. Kim, J. Moon, J. Kim, *J. Electrochem. Soc.* **2011**, *158*, A736-A740.
[111] H. F. Xiang, D. W. Zhang, Y. Jin, C. H. Chen, J. S. Wu, H. H. Wang, *J. Mater. Sci.* **2011**, *46*, 4906-4912.
[112] S. L. Yang, X. F. Zhou, J. G. Zhang, Z. P. Liu, *J. Mater. Chem.* **2010**, *20*, 8086-8091.
[113] K. Saravanan, M. V. Reddy, P. Balaya, H. Gong, B. V. R. Chowdari, J. J. Vittal, *J. Mater. Chem.* **2009**, *19*, 605-610.
[114] K. Saravanan, P. Balaya, M. V. Reddy, B. V. R. Chowdari, J. J. Vittal, *Energy & Environmental Science* **2010**, *3*, 457-464.
[115] P. Balaya, K. Saravanan, S. Hariharan, in *Energy Harvesting and Storage: Materials, Devices, and Applications, Vol. 7683* (Eds.: N. K. Dhar, P. S. Wijewarnasuriya, A. K. Dutta), Spie-Int Soc Optical Engineering, Bellingham, **2010**.
[116] Z. Y. Bi, X. D. Zhang, W. He, D. D. Min, W. S. Zhang, *Rsc Adv* **2013**, *3*, 19744-19751.
[117] K. T. Lee, J. Cho, *Nano Today* **2011**, *6*, 28-41.
[118] C. M. Julien, A. Mauger, K. Zaghib, *J. Mater. Chem.* **2011**, *21*, 9955-9968.
[119] W. J. Zhang, *J. Electrochem. Soc.* **2010**, *157*, A1040-A1046.
[120] X. Zhao, B. M. Sanchez, P. J. Dobson, P. S. Grant, *Nanoscale* **2011**, *3*, 839-855.
[121] D. Zhang, R. Cai, Y. K. Zhou, Z. P. Shao, X. Z. Liao, Z. F. Ma, *Electrochim. Acta* **2010**, *55*, 2653-2661.
[122] Y. G. Wang, Y. R. Wang, E. J. Hosono, K. X. Wang, H. S. Zhou, *Angew. Chem.-Int. Edit.* **2008**, *47*, 7461-7465.
[123] S. Y. Lim, C. S. Yoon, J. P. Cho, *Chem. Mater.* **2008**, *20*, 4560-4564.
[124] M. Konarova, I. Taniguchi, *J. Power Sources* **2010**, *195*, 3661-3667.
[125] J. J. Wang, J. L. Yang, Y. J. Tang, J. Liu, Y. Zhang, G. X. Liang, M. Gauthier, Y. C. K. Chen-Wiegart, M. N. Banis, X. F. Li, R. Y. Li, J. Wang, T. K. Sham, X. L. Sun, *Nat Commun* **2014**, *5*.
[126] B. Kang, G. Ceder, *Nature* **2009**, *458*, 190-193.
[127] F. Yu, S. G. Ge, B. Li, G. Z. Sun, R. G. Mei, L. X. Zheng, *Current Inorganic Chemistry* **2012**, *2*, 194-212.
[128] F. Cheng, Z. Tao, J. Liang, J. Chen, *Chem. Mater.* **2008**, *20*, 667-681.
[129] M. R. Hill, G. J. Wilson, L. Bourgeois, A. G. Pandolfo, *Energy & Environmental Science* **2011**, *4*, 965-972.
[130] L. Dimesso, C. Forster, W. Jaegermann, J. P. Khanderi, H. Tempel, A. Popp, J. Engstler, J. J. Schneider, A. Sarapulova, D. Mikhailova, L. A. Schmitt, S. Oswald, H. Ehrenberg, *Chemical Society Reviews* **2012**, *41*, 5068-5080.
[131] X. D. Zhang, X. G. Zhang, W. He, C. Y. Sun, J. Y. Ma, J. L. Yuan, X. Y. Du, *Colloid Surface B* **2013**, *103*, 114-120.
[132] Y. Ma, X. L. Li, S. F. Sun, X. P. Hao, Y. Z. Wu, *Int J Electrochem Sc* **2013**, *8*, 2842-2848.
[133] J. F. Qian, M. Zhou, Y. L. Cao, X. P. Ai, H. X. Yang, *J. Phys. Chem. C* **2010**, *114*, 3477-3482.
[134] X. Qin, X. H. Wang, H. M. Xiang, J. Xie, J. J. Li, Y. C. Zhou, *J. Phys. Chem. C* **2010**, *114*, 16806-16812.
[135] D. G. Tong, Y. L. Li, W. Chu, P. Wu, F. L. Luo, *Dalton Trans.* **2011**, *40*, 4087-4094.
[136] D. W. Han, W. H. Ryu, W. K. Kim, S. J. Lim, Y. I. Kim, J. Y. Eom, H. S. Kwon, *Acs Appl Mater Inter* **2013**, *5*, 1342-1347.
[137] A. Carné-Sánchez, I. Imaz, M. Cano-Sarabia, D. Maspoch, *Nat Chem* **2013**, *5*, 203-211.
[138] F. Yu, J. J. Zhang, Y. F. Yang, G. Z. Song, *Journal of Materials Chemistry* **2009**, *19*, 9121-9125.
[139] S. Yu, S. Kim, T. Y. Kim, J. H. Nam, W. I. Cho, *J. Appl. Electrochem.* **2013**, *43*, 253-262.
[140] F. Yu, J. J. Zhang, Y. F. Yang, G. Z. Song, *J. Power Sources* **2009**, *189*, 794-797.
[141] J. Liu, T. E. Conry, X. Y. Song, M. M. Doeff, T. J. Richardson, *Energy & Environmental Science* **2011**, *4*, 885-888.
[142] B. F. Zou, Y. Q. Wang, S. M. Zhou, *Mater. Lett.* **2013**, *92*, 300-303.
[143] W. Chang, S. J. Kim, I. T. Park, B. W. Cho, K. Y. Chung, H. C. Shin, *J. Alloys Compd.* **2013**, *563*, 249-253.
[144] X. H. Rui, Y. Jin, X. Y. Feng, L. C. Zhang, C. H. Chen, *J. Power Sources* **2011**, *196*, 2109-2114.
[145] H. Q. Li, H. S. Zhou, *Chem. Commun.* **2012**, *48*, 1201-1217.
[146] D. Zane, M. Carewska, S. Scaccia, F. Cardellini, P. P. Prosini, *Electrochim. Acta* **2004**, *49*, 4259-4271.
[147] S. Xin, Y. G. Guo, L. J. Wan, *Accounts of Chemical Research* **2012**, *45*, 1759-1769.
[148] J. J. Wang, X. L. Sun, *Energy & Environmental Science* **2012**, *5*, 5163-5185.
[149] F. Y. Kang, J. Ma, B. H. Li, *New Carbon Mater.* **2011**, *26*, 161-170.
[150] M. Inagaki, *Carbon* **2012**, *50*, 3247-3266.
[151] Y. Zhou, C. D. Gu, J. P. Zhou, L. J. Cheng, W. L. Liu, Y. Q. Qiao, X. L. Wang, J. P. Tu, *Electrochim. Acta* **2011**, *56*, 5054-5059.
[152] X. D. Yan, G. L. Yang, J. Liu, Y. C. Ge, H. M. Xie, X. M. Pan, R. S. Wang, *Electrochim. Acta* **2009**, *54*, 5770-5774.
[153] S. W. Oh, S. T. Myung, S. M. Oh, K. H. Oh, K. Amine, B. Scrosati, Y. K. Sun, *Adv. Mater.* **2010**, *22*, 4842-4845.
[154] H. M. Xie, R. S. Wang, J. R. Ying, L. Y. Zhang, A. F. Jalbout, H. Y. Yu, G. L. Yang, X. M. Pan, Z. M. Su, *Adv. Mater.* **2006**, *18*, 2609-2613.
[155] L. J. Zeng, Q. Gong, X. Z. Liao, L. He, Y. S. He, Z. F. Ma, *Chin. Sci. Bull.* **2011**, *56*, 1262-1266.
[156] J. C. Zheng, X. H. Li, Z. X. Wang, J. H. Li, L. Wu, L. J. Li, H. J. Guo, *Acta Physico-Chimica Sinica* **2009**, *25*, 1916-1920.
[157] G. Yang, C. Y. Jiang, X. M. He, J. R. Ying, J. Gao, *Ionics* **2013**, *19*, 1247-1253.
[158] M. R. Yang, W. H. Ke, S. H. Wu, *J. Power Sources* **2007**, *165*, 646-650.
[159] L. Wu, J. J. Lu, S. K. Zhong, *Journal of Solid State Electrochemistry* **2013**, *17*, 2235-2241.
[160] J. C. Zheng, X. H. Li, Z. X. Wang, D. M. Qin, H. J. Guo, W. J. Peng, *J. Inorg. Mater.* **2009**, *24*, 143-146.
[161] Z. P. Ma, G. J. Shao, X. Wang, J. J. Song, G. L. Wang, *Ionics* **2013**, *19*, 1861-1866.
[162] X. Z. Liao, Z. F. Ma, Q. Gong, Y. S. He, L. Pei, L. J. Zeng, *Electrochem. Commun.* **2008**, *10*, 691-694.
[163] S. S. Zhang, K. Xu, T. R. Jow, *J. Power Sources* **2006**, *159*, 702-707.
[164] A. Yamada, S. C. Chung, K. Hinokuma, *J. Electrochem. Soc.* **2001**, *148*, A224-A229.
[165] Z. H. Li, D. M. Zhang, F. X. Yang, *J. Mater. Sci.* **2009**, *44*, 2435-2443.
[166] J. R. Ying, M. Lei, C. Y. Jiang, C. R. Wan, X. M. He, J. J. Li, L. Wang, J. G. Ren, *J. Power Sources* **2006**, *158*, 543-549.
[167] J. F. Ni, H. H. Zhou, J. T. Chen, X. X. Zhang, *Mater. Lett.* **2007**, *61*, 1260-1264.
[168] X. M. Lou, Y. X. Zhang, *J. Mater. Chem.* **2011**, *21*, 4156-4160.
[169] P. K. Shen, H. L. Zou, H. Meng, M. M. Wu, *Funct Mater Lett* **2011**, *4*, 209-215.
[170] Y. H. Yin, M. X. Gao, J. L. Ding, Y. F. Liu, L. K. Shen, H. G. Pan, *J. Alloys Compd.* **2011**, *509*, 10161-10166.
[171] Y. H. Yin, M. X. Gao, H. G. Pan, L. K. Shen, X. Ye, Y. F. Liu, P. S. Fedkiw, X. W. Zhang, *J. Power Sources* **2012**, *199*, 256-262.

[172] Z. P. Ma, G. J. Shao, W. Wang, C. Y. Zhang, *Asian J. Chem.* **2013**, *25*, 3579-3582.
[173] S. W. Oh, S. T. Myung, S. M. Oh, C. S. Yoon, K. Amine, Y. K. Sun, *Electrochim. Acta* **2010**, *55*, 1193-1199.
[174] Z. R. Chang, H. J. Lv, H. W. Tang, H. J. Li, X. Z. Yuan, H. J. Wang, *Electrochim. Acta* **2009**, *54*, 4595-4599.
[175] S. W. Oh, S. T. Myung, H. J. Bang, C. S. Yoon, K. Amine, Y. K. Sun, *Electrochem. Solid State Lett.* **2009**, *12*, A181-A185.
[176] J. K. Kim, *Crystengcomm* **2014**, *16*, 2818-2822.
[177] F. Yu, L. L. Zhang, M. Y. Zhu, Y. X. An, L. L. Xia, X. G. Wang, B. Dai, *Nano Energy* **2014**, *3*, 64-79.
[178] J. M. Tarascon, N. Recham, M. Armand, J. N. Chotard, P. Barpanda, W. Walker, L. Dupont, *Chem. Mater.* **2010**, *22*, 724-739.
[179] O. Toprakci, H. A. K. Toprakci, L. W. Ji, X. W. Zhang, *KONA Powder Part. J.* **2010**, 50-73.
[180] S. M. Oh, H. G. Jung, C. S. Yoon, S. T. Myung, Z. H. Chen, K. Amine, Y. K. Sun, *J. Power Sources* **2011**, *196*, 6924-6928.
[181] J. Wang, Z. B. Shao, H. Q. Ru, *Ceram Int* **2014**, *40*, 6979-6985.
[182] J. J. Tan, A. Tiwari, *Nanosci Nanotech Let* **2011**, *3*, 487-490.
[183] Y. Y. Liu, D. W. Liu, Q. F. Zhang, G. Z. Cao, *Journal of Materials Chemistry* **2011**, *21*, 9969-9983.
[184] D. Jugovic, M. Mitric, M. Kuzmanovic, N. Cvjeticanin, S. Skapin, B. Cekic, V. Ivanovski, D. Uskokovic, *J. Power Sources* **2011**, *196*, 4613-4618.
[185] C. Miao, J. Zhou, S. Q. Sun, X. Y. Wang, *Rare Metal Mat Eng* **2013**, *42*, 379-382.
[186] Y. Zhang, Q. Y. Huo, P. P. Du, L. Z. Wang, A. Q. Zhang, Y. H. Song, Y. Lv, G. Y. Li, *Synth. Met.* **2012**, *162*, 1315-1326.
[187] F. Yu, J. J. Zhang, Y. F. Yang, G. Z. Song, *Chin. J. Inorg. Chem.* **2009**, *25*, 42-46.
[188] J. P. Jegal, K. B. Kim, *J. Power Sources* **2013**, *243*, 859-864.
[189] J. L. Yang, J. J. Wang, Y. J. Tang, D. N. Wang, X. F. Li, Y. H. Hu, R. Y. Li, G. X. Liang, T. K. Sham, X. L. Sun, *Energy & Environmental Science* **2013**, *6*, 1521-1528.
[190] P. P. Prosini, M. Carewska, S. Scaccia, P. Wisniewski, M. Pasquali, *Electrochim. Acta* **2003**, *48*, 4205-4211.
[191] P. Jozwiak, J. E. Garbarczyk, M. Wasiucionek, I. Gorzkowska, F. Gendron, A. Mauger, C. M. Julien, *Solid State Ionics* **2008**, *179*, 46-50.
[192] L. Yang, L. F. Jiao, Y. L. Miao, H. T. Yuan, *J. Solid State Electrochem.* **2009**, *13*, 1541-1544.
[193] J. Liu, J. W. Wang, X. D. Yan, X. F. Zhang, G. L. Yang, A. F. Jalbout, R. S. Wang, *Electrochim. Acta* **2009**, *54*, 5656-5659.
[194] C. W. Kim, M. H. Lee, W. T. Jeong, K. S. Lee, *J. Power Sources* **2005**, *146*, 534-538.
[195] C. W. Kim, J. S. Park, K. S. Lee, *J. Power Sources* **2006**, *163*, 144-150.
[196] K. T. Lee, K. S. Lee, *J. Power Sources* **2009**, *189*, 435-439.
[197] Y. B. Xu, Y. J. Lu, L. Yan, Z. Y. Yang, R. D. Yang, *J. Power Sources* **2006**, *160*, 570-576.
[198] S. B. Lee, S. H. Cho, S. J. Cho, G. J. Park, S. H. Park, Y. S. Lee, *Electrochem. Commun.* **2008**, *10*, 1219-1221.
[199] M. Hermanek, R. Zboril, M. Mashlan, L. Machala, O. Schneeweiss, *Journal of Materials Chemistry* **2006**, *16*, 1273-1280.
[200] W. Ojczyk, J. Marzec, K. Swierczek, W. Zajac, M. Molenda, R. Dziembaj, J. Molenda, *J. Power Sources* **2007**, *173*, 700-706.
[201] H. Liu, J. Y. Xie, K. Wang, *Solid State Ionics* **2008**, *179*, 1768-1771.
[202] H. W. Liu, D. G. Tang, *Solid State Ionics* **2008**, *179*, 1897-1901.
[203] Y. Lin, J. B. Wu, Y. B. Yu, in *Multi-Functional Materials and Structures Iii, Pts 1 and 2, Vol. 123-125*, Trans Tech Publications Ltd, Stafa-Zurich, **2010**, pp. 1227-1230.
[204] M. X. Gao, Y. Lin, Y. H. Yin, Y. F. Liu, H. G. Pan, *Electrochim. Acta* **2010**, *55*, 8043-8050.
[205] M. Konarova, I. Taniguchi, *Mater. Res. Bull.* **2008**, *43*, 3305-3317.
[206] M. Konarova, I. Taniguchi, *J. Power Sources* **2009**, *194*, 1029-1035.
[207] Y. Lin, M. X. Gao, D. Zhu, Y. F. Liu, H. G. Pan, *J. Power Sources* **2008**, *184*, 444-448.
[208] G. Arnold, J. Garche, R. Hemmer, S. Strobele, C. Vogler, A. Wohlfahrt-Mehrens, *J. Power Sources* **2003**, *119*, 247-251.
[209] Y. Z. Dong, Y. M. Zhao, H. Duan, L. Chen, Z. F. He, Y. H. Chen, *J. Solid State Electrochem.* **2010**, *14*, 131-137.
[210] S. Balaji, D. Mutharasu, N. Sankara Subramanian, K. Ramanathan, *Ionics* **2009**, *15*, 765-777.
[211] K. Cherian, *Adv Mater Process* **2011**, *169*, 23-27.
[212] X. F. Guo, H. Zhan, Y. H. Zhou, *Solid State Ionics* **2009**, *180*, 386-391.
[213] M. Higuchi, K. Katayama, Y. Azuma, M. Yukawa, M. Suhara, *J. Power Sources* **2003**, *119*, 258-261.
[214] M. S. Song, Y. M. Kang, J. H. Kim, H. S. Kim, D. Y. Kim, H. S. Kwon, J. Y. Lee, *J. Power Sources* **2007**, *166*, 260-265.
[215] M. S. Song, Y. M. Kang, Y. I. Kim, K. S. Park, H. S. Kwon, *Inorg. Chem.* **2009**, *48*, 8271-8275.
[216] K. S. Park, J. T. Son, H. T. Chung, S. J. Kim, C. H. Lee, H. G. Kim, *Electrochem. Commun.* **2003**, *5*, 839-842.
[217] H. L. Zou, G. H. Zhang, P. K. Shen, *Mater. Res. Bull.* **2010**, *45*, 149-152.
[218] L. Wang, Y. D. Huang, R. R. Jiang, D. Z. Jia, *Electrochim. Acta* **2007**, *52*, 6778-6783.
[219] L. Wang, Y. D. Huang, R. R. Jiang, D. Z. Jia, *J. Electrochem. Soc.* **2007**, *154*, A1015-A1019.
[220] D. Li, Y. D. Huang, N. Sharma, Z. X. Chen, D. Z. Jia, Z. P. Guo, *PCCP* **2012**, *14*, 3634-3639.
[221] D. Li, Y. D. Huang, D. Z. Jia, Z. P. Guo, S. J. Bao, *J. Solid State Electrochem.* **2010**, *14*, 889-895.
[222] Y. Zhang, H. Feng, X. B. Wu, L. Z. Wang, A. Q. Zhang, T. C. Xia, H. C. Dong, M. H. Liu, *Electrochim. Acta* **2009**, *54*, 3206-3210.
[223] X. F. Guo, Y. T. Zhang, H. Zhan, Y. H. Zhou, *Solid State Ionics* **2010**, *181*, 1757-1763.
[224] S. Feng, L. Guanghua, in *Modern Inorganic Synthetic Chemistry* (Eds.: X. Ruren, P. Wenqin, W. P. Qisheng HuoA2 - Ruren Xu, H. Qisheng), Elsevier, Amsterdam, **2011**, pp. 63-95.
[225] X. Q. Ou, S. Z. Xu, G. C. Liang, L. Wang, X. Zhao, *Sci China Ser E* **2009**, *52*, 264-268.
[226] M. K. Devaraju, I. Honma, *Adv Energy Mater* **2012**, *2*, 284-297.
[227] C. B. Xu, J. Lee, A. S. Teja, *J. Supercrit. Fluids* **2008**, *44*, 92-97.
[228] A. Aimable, D. Aymes, F. Bernard, F. Le Cras, *Solid State Ionics* **2009**, *180*, 861-866.
[229] N. Recham, L. Dupont, M. Courty, K. Djellab, D. Larcher, M. Armand, J. M. Tarascon, *Chem. Mater.* **2009**, *21*, 1096-1107.
[230] N. Recham, J. N. Chotard, L. Dupont, K. Djellab, M. Armand, J. M. Tarascon, *J. Electrochem. Soc.* **2009**, *156*, A993-A999.
[231] P. Barpanda, N. Recham, J. N. Chotard, K. Djellab, W. Walker, M. Armand, J. M. Tarascon, *J. Mater. Chem.* **2010**, *20*, 1659-1668.
[232] M. C. Tucker, M. M. Doeff, T. J. Richardson, R. Finones, J. A. Reimer, E. J. Cairns, *Electrochem. Solid State Lett.* **2002**, *5*, A95-A98.
[233] K. Shiraishi, K. Dokko, K. Kanamura, *J. Power Sources* **2005**, *146*, 555-558.
[234] K. Dokko, S. Koizumi, K. Sharaishi, K. Kanamura, *J. Power Sources* **2007**, *165*, 656-659.
[235] K. Kanamura, S. H. Koizumi, K. R. Dokko, *J. Mater. Sci.* **2008**, *43*, 2138-2142.
[236] K. Dokko, S. Koizumi, K. Kanamura, *Chem. Lett.* **2006**, *35*, 338-339.
[237] S. F. Yang, P. Y. Zavalij, M. S. Whittingham, *Electrochem. Commun.* **2001**, *3*, 505-508.
[238] M. Koltypin, D. Aurbach, L. Nazar, B. Ellis, *J. Power Sources* **2007**, *174*, 1241-1250.

[239] S. Franger, F. Le Cras, C. Bourbon, H. Rouault, *Electrochem. Solid State Lett.* **2002**, *5*, A231-A233.
[240] J. L. Liu, R. R. Jiang, X. Y. Wang, T. Huang, A. S. Yu, *J. Power Sources* **2009**, *194*, 536-540.
[241] J. Chen, S. Wang, M. S. Whittingham, *J. Power Sources* **2007**, *174*, 442-448.
[242] J. J. Chen, M. S. Whittingham, *Electrochem. Commun.* **2006**, *8*, 855-858.
[243] X. Q. Ou, H. C. Gu, Y. C. Wu, J. W. Lu, Y. J. Zheng, *Electrochim. Acta* **2013**, *96*, 230-236.
[244] R. G. Mei, X. R. Song, Y. F. Yang, Z. G. An, J. J. Zhang, *Rsc Advances* **2014**, *4*, 5746-5752.
[245] J. Lee, A. S. Teja, *J. Supercrit. Fluids* **2005**, *35*, 83-90.
[246] K. Dokko, S. Koizumi, H. Nakano, K. Kanamura, *J. Mater. Chem.* **2007**, *17*, 4803-4810.
[247] J. J. Chen, M. J. Vacchio, S. J. Wang, N. Chernova, P. Y. Zavalij, M. S. Whittingham, *Solid State Ionics* **2008**, *178*, 1676-1693.
[248] Y. Xia, W. K. Zhang, H. Huang, Y. P. Gan, J. Tian, X. Y. Tao, *J. Power Sources* **2011**, *196*, 5651-5658.
[249] J. F. Ni, M. Morishita, Y. Kawabe, M. Watada, N. Takeichi, T. Sakai, *J. Power Sources* **2010**, *195*, 2877-2882.
[250] Z. G. Lu, H. L. Chen, R. Robert, B. Y. X. Zhu, J. Q. Deng, L. J. Wu, C. Y. Chung, C. P. Grey, *Chem. Mater.* **2011**, *23*, 2848-2859.
[251] G. Meligrana, C. Gerbaldi, A. Tuel, S. Bodoardo, N. Penazzi, *J. Power Sources* **2006**, *160*, 516-522.
[252] C. Gerbaldi, J. Nair, C. B. Minella, G. Meligrana, G. Mulas, S. Bodoardo, R. Bongiovanni, N. Penazzi, *J. Appl. Electrochem.* **2008**, *38*, 985-992.
[253] S. Bodoardo, C. Gerbaldi, G. Meligrana, A. Tuel, S. Enzo, N. Penazzi, *Ionics* **2009**, *15*, 19-26.
[254] G. X. Wang, X. P. Shen, J. Yao, *J. Power Sources* **2009**, *189*, 543-546.
[255] Y. M. Jiang, S. J. Liao, Z. S. Liu, G. Xiao, Q. B. Liu, H. Y. Song, *J Mater Chem A* **2013**, *1*, 4546-4551.
[256] S. Tajimi, Y. Ikeda, K. Uematsu, K. Toda, M. Sato, *Solid State Ionics* **2004**, *175*, 287-290.
[257] Z. H. Xu, L. Xu, Q. Y. Lai, X. Y. Ji, *Mater. Res. Bull.* **2007**, *42*, 883-891.
[258] F. Teng, M. D. Chen, G. Q. Li, Y. Teng, T. G. Xu, S. I. Mho, X. Hua, *J. Power Sources* **2012**, *202*, 384-388.
[259] G. Yang, H. M. Ji, H. D. Liu, K. F. Huo, J. J. Fu, P. K. Chu, *J Nanosci Nanotechno* **2010**, *10*, 980-986.
[260] G. Yang, H. M. Ji, X. W. Miao, A. Q. Hong, Y. Yan, *J Nanosci Nanotechno* **2011**, *11*, 4781-4792.
[261] D. Carriazo, M. D. Rossell, G. B. Zeng, I. Bilecka, R. Erni, M. Niederberger, *Small* **2012**, *8*, 2231-2238.
[262] A. V. Murugan, T. Muraliganth, A. Manthiram, *J. Phys. Chem. C* **2008**, *112*, 14665-14671.
[263] A. V. Murugan, T. Muraliganth, A. Manthiram, *J. Electrochem. Soc.* **2009**, *156*, A79-A83.
[264] T. Muraliganth, A. V. Murugan, A. Manthiram, *J. Mater. Chem.* **2008**, *18*, 5661-5668.
[265] A. V. Murugan, T. Muraliganth, P. J. Ferreira, A. Manthiram, *Inorg. Chem.* **2009**, *48*, 946-952.
[266] A. V. Murugan, T. Muraliganth, A. Manthiram, *Electrochem. Commun.* **2008**, *10*, 903-906.

Figures

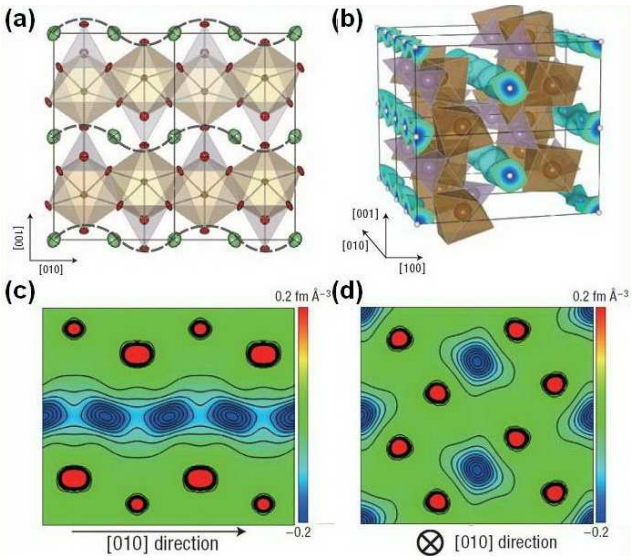

Figure 1 (a) Anisotropic harmonic lithium vibration in $LiFePO_4$ shown as green thermal ellipsoids and the expected curved one-dimensional diffusion pathway (Dashed lines show how the motions of Li atoms evolve from vibrations to diffusion) (b) Three-dimensional Li nuclear density data shown as blue contours. The brown octahedra represent FeO_6 and the purple tetrahedral represent PO_4 units. (Equi-value 0.15 fm·$Å^{-3}$ of the negative portion of the coherent nuclear scattering density distribution) (c) Two-dimensional contour map sliced on the (001) plane at z =0.5 and (d) the (010) plane at y =0, whereas Fe, P and O atoms remain near their original positions. [40]

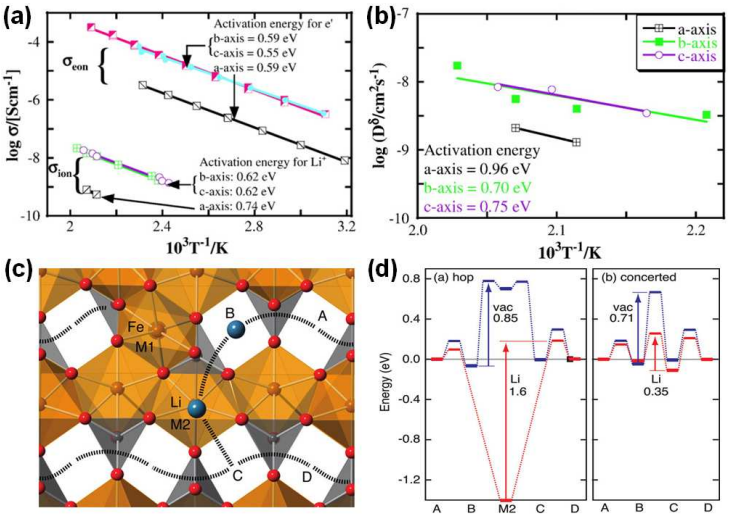

Figure 2 (a) Comparison of ionic and electronic conductivities along different along different crystallographic orientations. (b) Chemical diffusion coefficient along different directions.[47] (c) For the anti-site defect shown, Fe sits in the channel at site M1 and Li sits in the $FePO_4$ lattice at site M2. Dashed lines represent the diffusion pathways for Li ions in the lattice. (d) Energy landscape for diffusion around the defect resulting in cross-channel diffusion of Li ions (red) and vacancies (blue).[49]

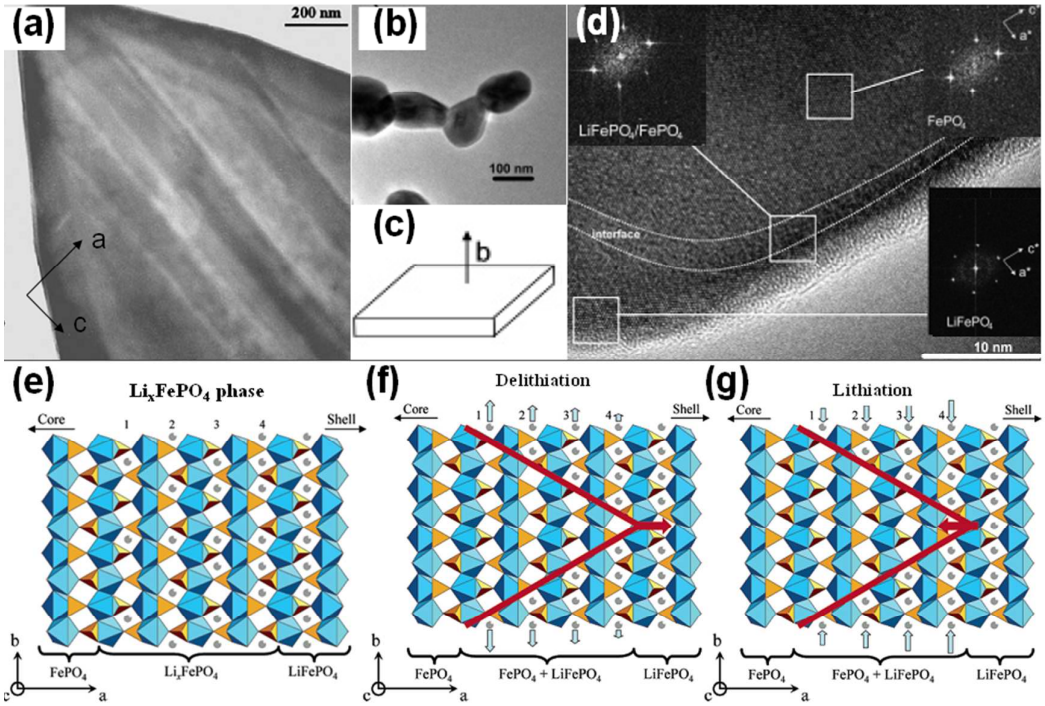

Figure 3 (a) TEM image of a $Li_{0.5}FePO_4$ crystal, showing the domains of $LiFePO_4$ and $FePO_4$ aligned along the c-axis.[60] (b) TEM and (d) HRTEM images of the delithiated $Li_{0.45}FePO_4$ sample. The phase determination present in the edge, core, or interface of the particle, respectively. (c) Sketch of the $Li_{0.45}FePO_4$ particle. (e,f,g) Schematic views of the interfacial region between LiFePO4 and FePO4 phases.[51]

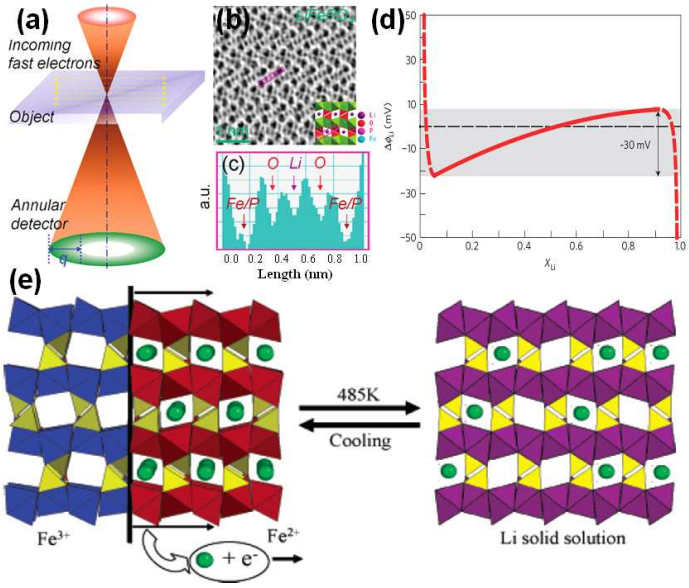

Figure 4 (a) Schematic of the annular-bright-field (ABF) imaging geometry. A demonstration of lithium sites within a $LiFePO_4$ crystal is shown in (b) with the corresponding line profile acquired at the box region shown in (c) to confirm the lithium contrast with respect to oxygen.[77] (d) The single-particle voltage within $0.5<x<0.9$ in Li_xFePO_4.[78] (e) Illustration of a solid solution Li_xFePO_4 upon heating the compound to 485 K. On cooling, the parent $LiFePO_4$ and $FePO_4$ phases recrystallize, and nucleation and growth take place everywhere within the crystal.[48]

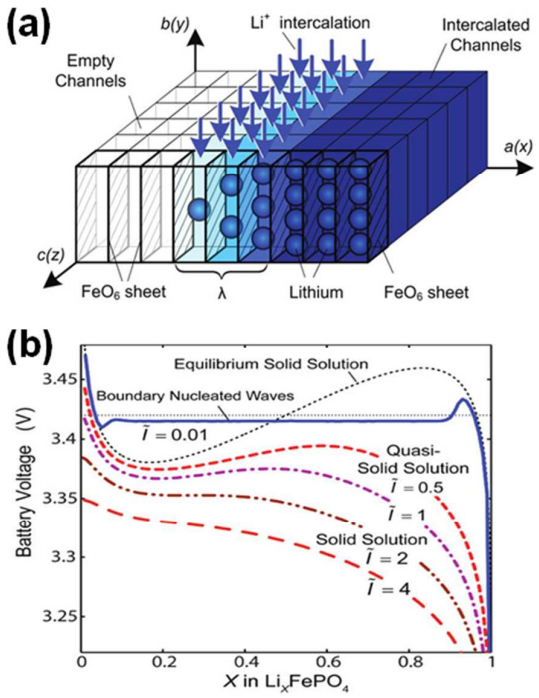

Figure 5 Schematic model of a Li_xFePO_4 nanoparticle at low overpotential. (a) Lithium ions are inserted into the particle (blue arrows) from the active (010) facet with fast diffusion and no phase separation in the depth (y) direction, forming a phase boundary of thickness λ between full and empty channels. (b) Numerical simulation of phase transformation triggered by wetting of the particle boundary.[80]

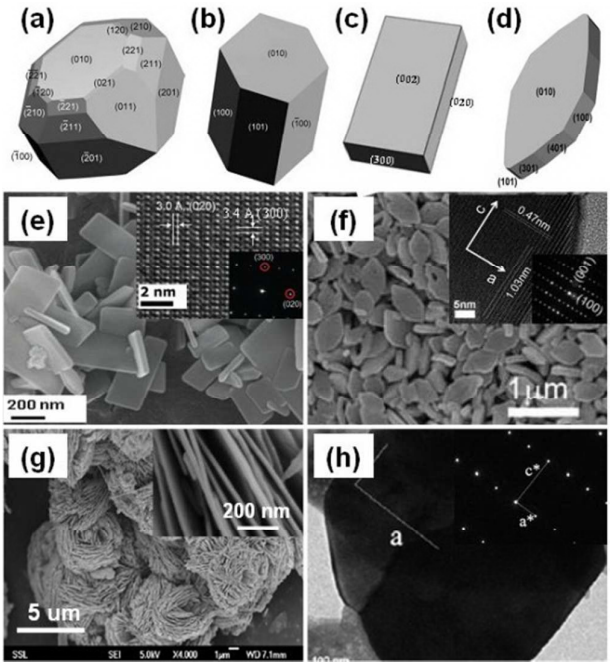

Figure 6 (a) Theoretical crystal morphologies of $LiFePO_4$ with equilibrium morphology from relaxed surface energies. Schematic diagrams of observed crystal morphologies of $LiFePO_4$ produced under different experimental conditions: (b) block-shape, (c) rectangular prism and (d) hexagonal platelet.[104] SEM morphology of (e) rectangular prism nanoplates,[110] (f) hexagonal platelet,[112] (g) SEM and (h) TEM morphologies of nanoplates.[113]

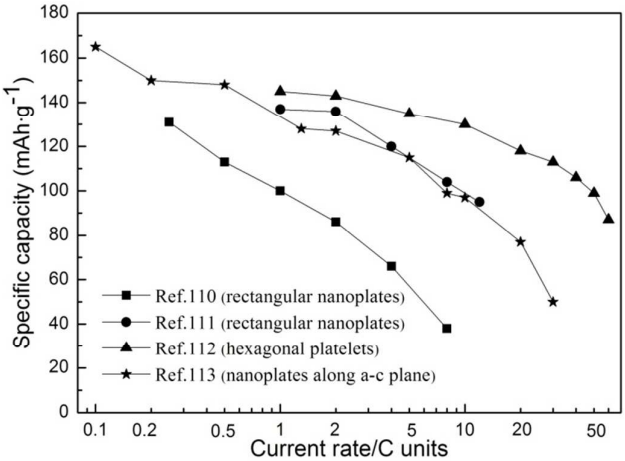

Figure 7 High rate capacity performance of $LiFePO_4$ particles with different observed crystal morphologies.

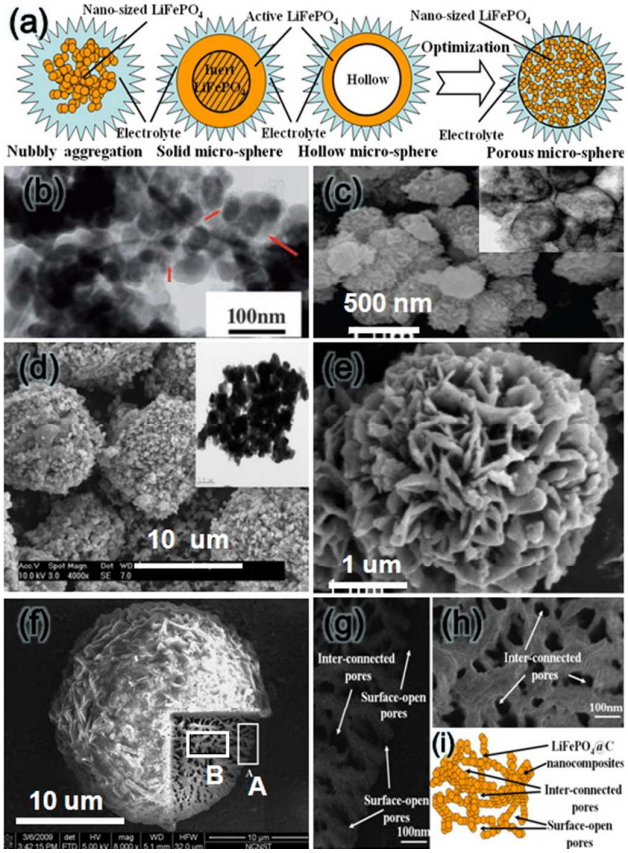

Figure 8 (a) Schematic illustration for active $LiFePO_4$ at different interfaces of electrolyte and various LiFePO4 particles.[138] (b) TEM image of $LiFePO_4$/C nanopaticles.[122] (c) SEM and TEM (inset) images of hollow $LiFePO_4$.[123] (d) SEM and TEM (inset) images of porous and coarse $LiFePO_4$/C composite.[136] (e) SEM image of an individual $LiFePO_4$/C microsphere consisted of nanoplates.[92] (f) FIB images allowing 3D visualization information obtained from the 3D porous $LiFePO_4$/C microsphere. (g) SEM image of A area (indicated by a rectangle in panel f). (g) SEM image of B area (indicated by a rectangle in panel f). (i) Scheme showing the structure of $LiFePO_4$/C nanocomposites in porous microspheres.[138]

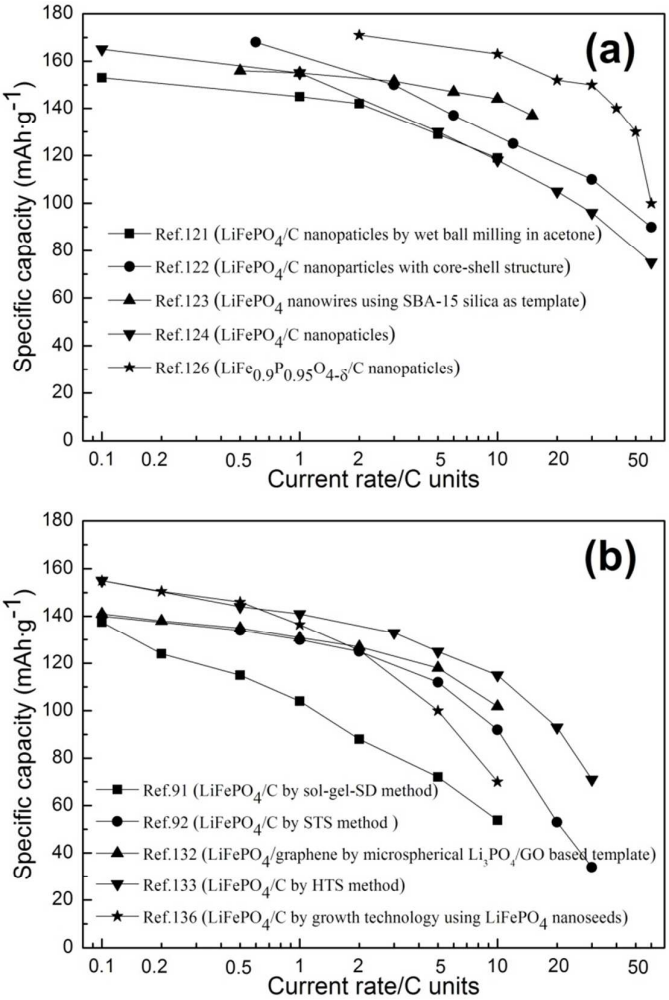

Figure 9 High rate capacity performance of $LiFePO_4$ particles with (a) nano-sized and (b) 3D porous morphologies.

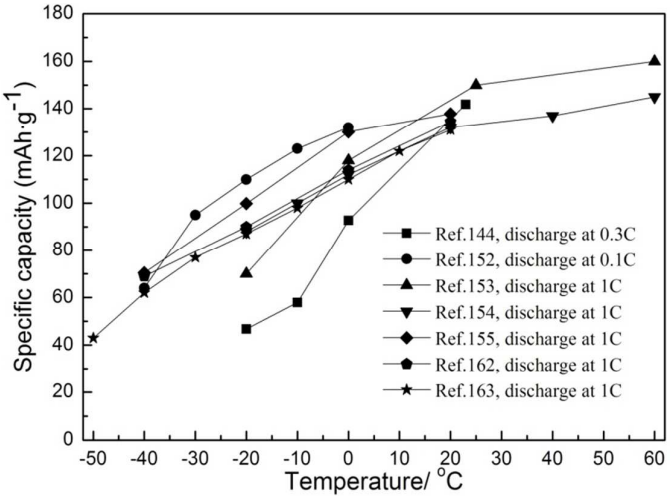

Figure 10 Rate capacity performance of $LiFePO_4$ at various temperature.

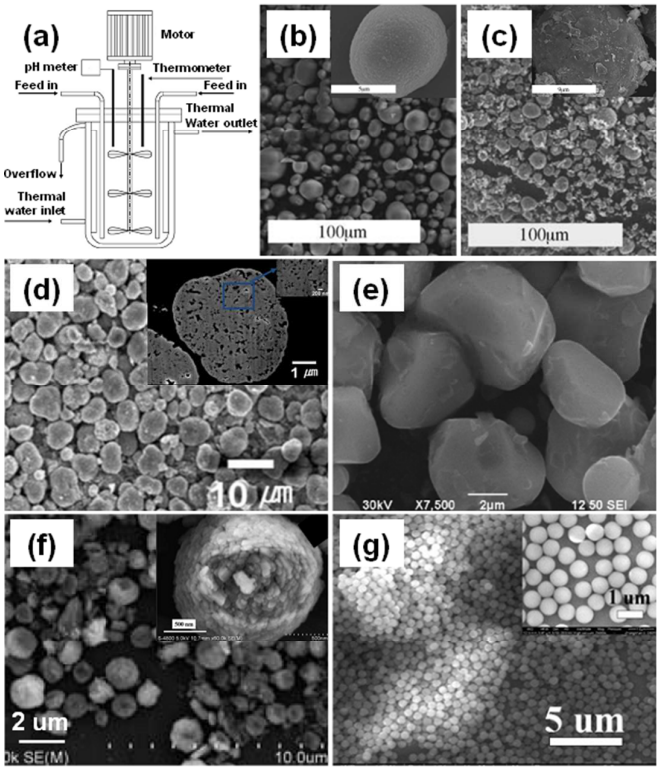

Figure 11 (a) Schematic diagram of the reactor for controlled crystallization process. The SEM images panorama and individual for (b) $FePO_4 \cdot xH_2O$ and (c) $Li_{0.97}Cr_{0.01}FePO_4/C$ particles prepared by controlled crystallization method.[166] (d) Porous spongelike $LiFePO_4$ and the corresponding cross-sectional SEM image (inset).[175] (e) SEM images of $LiFePO_4/C$ containing 7.0 wt.% carbon synthesized by coprecipitation method using self-produced high-density $FePO_4$ pressure-filtrated at 20 MPa.[174] (f) SEM image of quasi-spherical $FePO_4 \cdot 2H_2O$ precursor synthesizedby hydrothermal method.[168] (g) SEM micrographs of $LiFePO_4$ with quite a high tap density of 2.0 $g \cdot cm^{-3}$ obtained by microwave assisted water-bath reaction method.[169]

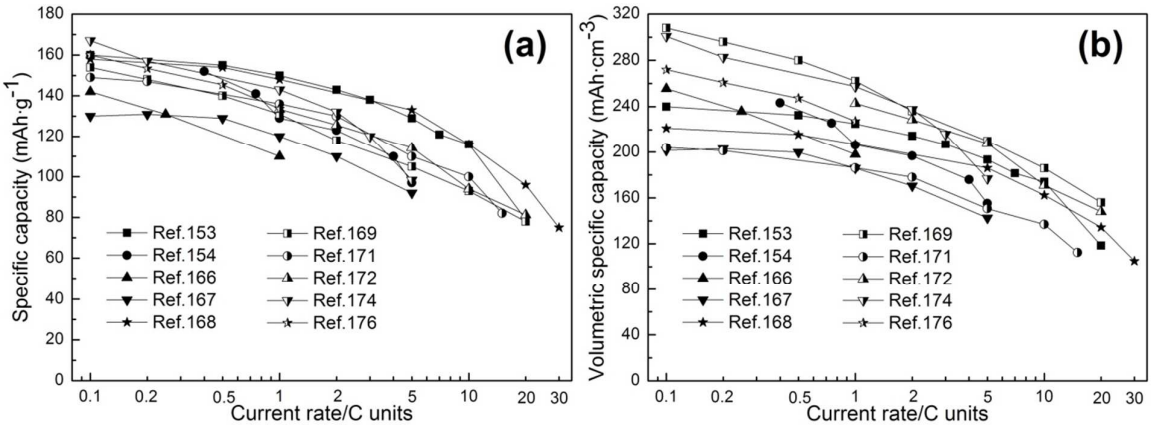

Figure 12 (a) Rate capacities for various samples and (b) their volumetric energy densities.

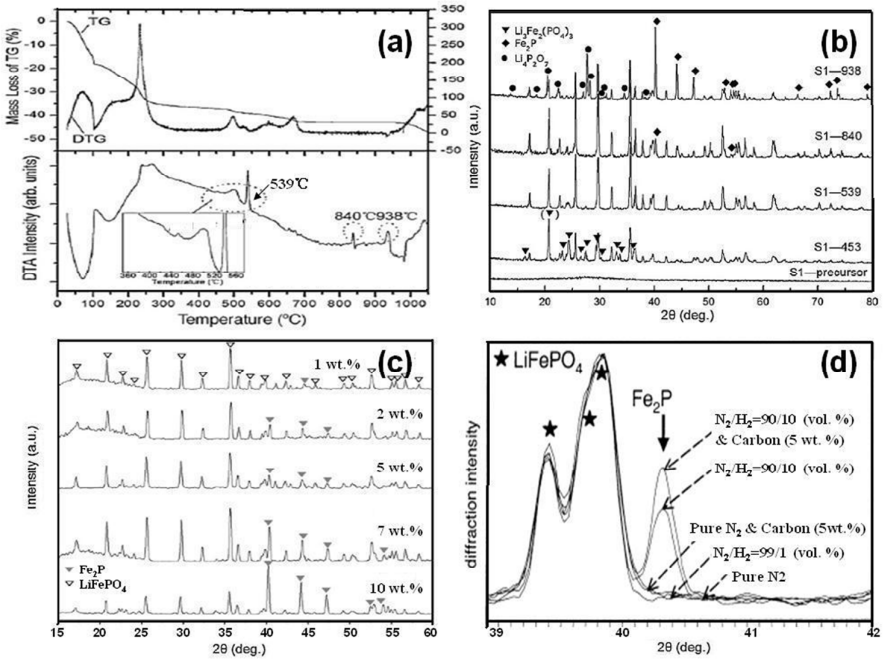

Figure 13 (a) TG-DTA curves of the Fe(III) precursor using carbon black as carbon sources, and (b) corresponding XRD patterns of the precursor and $LiFePO_4$/C samples after heating at various temperatures.[94] (c) XRD profiles of the $LiFePO_4/Fe_2P$ composites synthesized using different amounts of excess carbon.[195] (d) XRD patterns of samples prepared from a slightly oxidized Fe(II) precursor using various reductive heat treatments.[208]

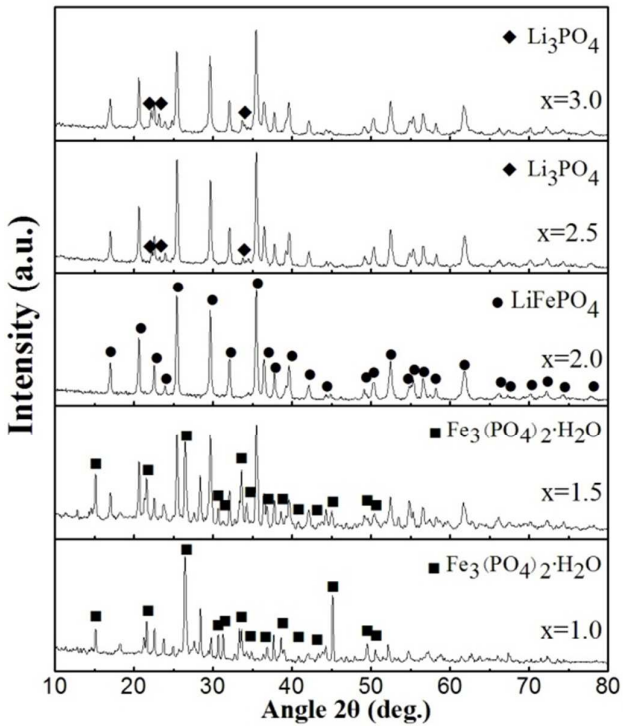

Figure 14 XRD patterns of the samples prepared by different value of x in molar ratio of x:1:1 for the starting materials including LiOH, $FeSO_4$ and $NH_4H_2PO_4$.

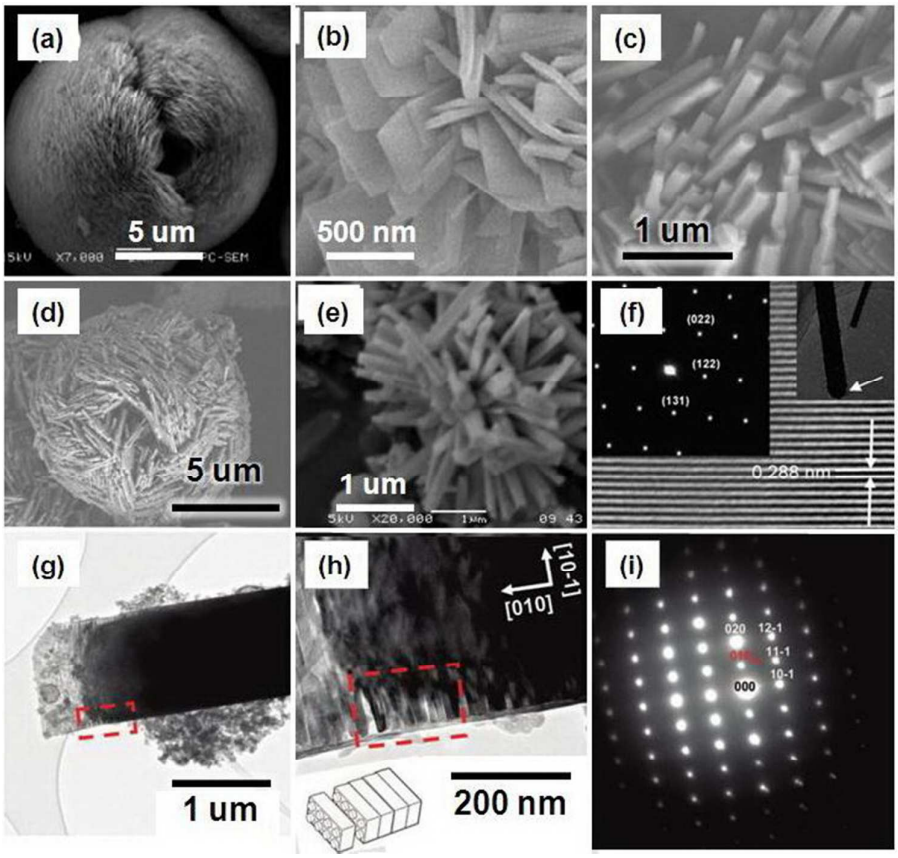

Figure 15 (a) SEM images of a $LiFePO_4$ hemisphere, demonstrating the microsphere consisting of nanofibers.[255] (b) SEM images of $LiFePO_4$.[111] (c and d) SEM images of a $LiFePO_4$ hemisphere, and the $LiFePO_4$ nanorods. (e and f) SEM and HRTEM images of the LiFePO4 nanorods.[258] (g,h,i) TEM images of the large $LiFePO_4$ needle assembling of Lego blocks, and the corresponding SAED pattern. The white arrow shows the "cementing" zone.[229]

Tables

Table 1 Various $LiFePO_4$ and the corresponding electrolyte responsible for the excellent low-temperature performance.

Materials	Synthesis method	Low temperature range/^{o}C	Eleytrolye	Ref.
$LiFePO_4$/C	solid state reaction method	-20	1M $LiPF_6$/EC+DEC (1:1)	[144]
$LiFePO_4$/C	solid state reaction method	-20	1M $LiPF_6$/EC+DEC (1:1)	[151]
$LiFePO_4$/C	solid state reaction method	-40	1M $LiPF_6$/EC+DEC (1:1)	[152]
$LiFePO_4$/C	co-precipitation method	-20	1M $LiPF_6$/EC+DEC (1:1)	[153]
$LiFePO_4$/PAS	co-precipitation method	-20	1M $LiPF_6$/EC+DEC (1:1)	[154]
$LiFe_{0.98}Mn_{0.02}PO_4$/C	solid state reaction method	-40	1M $LiPF_6$/EC+DEC (1:1)	[155]
$LiFePO_4$/C	solid state reaction method	-40	1M $LiPF_6$/EC+DEC+DMC+EMC(1:1:1:3)	[162]
$LiFePO_4$/C	solid state reaction method	-50	1M(0.9$LiBF_4$+0.1LiBOB)/PC+EC+EMC(1:1:3)	[163]

Table 2 various samples with high volumetric energy density

Materials	Synthesis methods	Tap density($g^3 \cdot cm^{-3}$)	Ref.
$LiFePO_4/Fe_2P$	Ball milling	1.37	[170,171]
$LiFePO_4$/C	Ball milling	1.82	[172]
$Li_{0.97}Cr_{0.01}FePO_4$/C	Controlled crystallization method	1.8	[166]
$LiFePO_4$/PAS	Controlled crystallization method	1.6	[154]
$LiFePO_4$/C	Co-precipitation method	1.5-1.6	[153,173,175]
$LiFePO_4$/C	Co-precipitation method	1.8	[174]
$LiFePO_4$	Molten-salt method	1.55	[167]
$LiFePO_4$/C	Hydrothermal method	1.4	[168]
$LiFePO_4$	Spray drying method	1.7	[176]
$LiFePO_4$	Microwave assisted water-bath reaction	2.0	[169]

Table 3 Reaction mechanism of deoxidization reaction of $LiFePO_4$ in various conditions.

Reduction Condition	Chemical Reaction Equation	Ref.
Self-deoxidization reaction of $LiFePO_4$/C composite (at 840 ℃)	$4LiFePO_4$+7C (or 14C) =$2Fe_2P$+$2Li_2O$+2P+7CO_2 (or 14CO)	[94,195]
Severe decomposition of $LiFePO_4$/C composite (at 938 ℃)	$4LiFePO_4$+C (or 2C) =$2Fe_2P$+$2Li_4P_2O_7$+P+CO_2 (or 2CO)	[94]
Reducing agents (Fe_3O_4, Fe_3C, Fe nanoparticles) from $FeC_2O_4 \cdot 2H_2O$ (at 675 ℃)	$8FeC_2O_4 \cdot 2H_2O$+$4LiFePO_4$+24C (or 48C)=$4Fe_2P$+ $16H_2O$+24CO_2 (or 48CO)	[199,200]
Reducing agent iron nanoparticles		[202]
Reductive H_2 atmosphere	8Fe+$4LiFePO_4$+7C (or 14C) =$4Fe_2P$+$2Li_2O$+7CO_2 (or 14CO)	[99]
microwave assisted reaction	$6LiFePO_4$+$16H_2$ =$2Fe_2P$ + $2Li_3PO_4$ + 2FeP + $16H_2O$	[215]
microwave assisted reaction (without atmosphere of inert gases)	$8LiFePO_4$ =$2Li_4P_2O_7$ +$4Fe_2P$ +$9O_2$ $12LiFePO_4$+$3O_2$ =$4Li_3Fe_2(PO_4)_3$ +$2Fe_2O_3$	[213,222]

Table 4 Summary of representative reaction mechanism of $LiFePO_4$ prepared by low-temperatured LPT synthesis. In the table, mediator includes organic acids or surfactant compounds.

Synthesis type	Reaction reagents	Stoichiometric ratio	Mediator	Solvent	Condition	Morphology	Ref.
HTS	LiOH, $FeSO_4$, H_3PO_4	3:1:1	-	H_2O	120 °C,5 h	hexagonal platelets	[232]
HTS	LiOH, $FeSO_4$, $(NH_4)_3PO_4$	2.5:1:1	-	H_2O	170 °C, 12 h	-	[233]
HTS	LiOH, $FeSO_4$, $(NH_4)_2HPO_4$	1:1:1&2:1:1	-	H_2O	170 °C, 12 h	nanoplates	[234]
HTS	LiOH, $FeSO_4$, $NH_4H_2PO_4$	2:1:1	-	H_2O	180 °C, 5 h	spindle-like particles	This work
HTS	LiOH, $FeCl_2 \cdot 4H_2O$, P_2O_5	6:3:2	-	H_2O	170 °C, 3 days	hexagonal platelets	[237]
HTS	LiOH, $FeSO_4$, H_3PO_4	3:1:1	CTAB	H_2O	120 °C,5 h	nanoparticles	[251,252,253]
HTS	LiOH, $(NH_4)_2Fe(SO_4)_2 \cdot 6H_2O$, H_3PO_4	3:1:1	P123, D230	H_2O	220 °C,24 h	nanoparticles	[106]
HTS	LiOH, $(NH_4)_2Fe(SO_4)_2 \cdot 6H_2O$, H_3PO_4	3:1:1	Citric acid	H_2O	180 °C, 10 h	spindle-like particles	[250]
HTS	LiOH, $FeSO_4$, $NH_4H_2PO_4$	2:1:1	NTA	H_2O	180 °C, 20 h	nanowires	[254]
HTS	LiAc , $FeCl_3$, $NH_4H_2PO_4$	1:1:1	SDS+EN	H_2O	180 °C, 10 h	spheres assembled from nanorods	This work
STS	LiOH, $FeSO_4$, H_3PO_4	3:1:1	-	TEG+H_2O	190 °C, 5 h	rectangular nanoplatelets	[111]
STS	LiOH, $FeSO_4$, H_3PO_4	3:1:1	Citric acid	MPG+H_2O	140 °C,12 h	needles asssembled nanorods	[255]
STS	LiOH, $FeSO_4$, H_3PO_4	3:1:1	-	PEG400+H_2O	150 °C,3 h	needle-like particles	[256]
STS	LiOH, $FeSO_4$, H_3PO_4	3:1:1	-	PEG400+H_2O	180 °C, 9 h	hexagonal platelet	[112]
ITS	LiH_2PO_4, $FeC_2O_4 \cdot 2H_2O$	1:1	-	CN-based IL	250 °C, 24 h	needles asssembled Lego blocks	[229]
ITS	LiOH, $FeSO_4$, H_3PO_4	3:1:1	SDBS+Ascorbic acid	IL+H_2O	240 °C, 20 h	nanorods	[258]
MW-HTS	LiOH, $FeSO_4$, H_3PO_4	3:1:1	-	H_2O	200 °C, 5 min	globular particles	[259]

MW-STS	LiOH, $FeAc_2$, H_3PO_4	1:1:1	-	TEG	300 ^oC, 5 min	nanorods	[262]